NASA Technical Memorandum 81940

CHARACTERIZATION OF DELAMINATION ONSET AND GROWTH IN A COMPOSITE LAMINATE

T. Kevin O'Brien

January 1981

NASA
National Aeronautics and
Space Administration
Langley Research Center
Hampton, Virginia 23665

DISCLAIMER NOTICE

THIS DOCUMENT IS BEST QUALITY AVAILABLE. THE COPY FURNISHED TO DTIC CONTAINED A SIGNIFICANT NUMBER OF PAGES WHICH DO NOT REPRODUCE LEGIBLY.

CHARACTERIZATION OF DELAMINATION ONSET AND GROWTH IN A COMPOSITE LAMINATE

T. Kevin O'Brien
Structures Laboratory
U.S. Army Research and Technology Laboratories (AVRADCOM)
NASA Langley Research Center
Hampton, Virginia 23665

SUMMARY

The onset and growth of delaminations in unnotched $[\pm 30/\pm 30/90/\overline{90}]_s$ graphite-epoxy laminates is described quantitatively. These laminates, designed to delaminate at the edges under tensile loads, were tested and analyzed. Delamination growth and stiffness loss were monitored nondestructively. Laminate stiffness decreased linearly with delamination size. The strain energy release rate, G, associated with delamination growth, was calculated from two analyses. A critical G for delamination onset was determined, and then was used to predict the onset of delaminations in $[+45_n/-45_n/0_n/90_n]_s$ (n=1,2,3) laminates. A delamination resistance curve (R-curve) was developed to characterize the observed stable delamination growth under quasi-static loading. A power law correlation between G and delamination growth rates in fatigue was established.

INTRODUCTION

A commonly observed failure mode in laminated composite materials is delamination between the composite layers. Delaminations may develop during manufacture due to incomplete curing or the introduction of a foreign particle; they may result from impact damage; or they may result from the interlaminar stresses that develop at stress-free edges or discontinuities. Furthermore, delaminations may grow under cyclic loading. Delamination growth redistributes the stresses in the plies of a laminate, and may influence residual stiffness, residual strength, and fatigue life. Hence, a fatigue analysis for composite materials should take into account the presence and growth of delaminations.

A bibliography of experimental and analytical work on delamination is contained in reference [1]. One of the most promising techniques for characterizing delamination growth is based on the rate of strain energy released, G, with delamination growth [1]. Previous work [2] has shown that the cyclic growth rate of debonds between the metal and composite components of reinforced panels could be correlated with G. Measured critical G values have been used in sophisticated analyses [3,4] to predict the onset of edge delaminations in unnotched composite laminates.

In the present study, a simple technique was developed, employing strain energy release rates to characterize the onset and growth of delaminations in a composite laminate. First, the damage that developed in unnotched $[\pm 30/\pm 30/90/\overline{90}]_s$ graphite-epoxy laminates under static tension loading and tension-tension fatigue loading was determined. Next, stress distributions generated from a finite element analysis were correlated with the observed damage. Then, during quasi-static test

loads, delamination growth and stiffness loss were monitored nondestructively to relate laminate stiffness and delamination size. The resulting test data and analysis were used to derive a closed-form equation for the strain energy release rate, G, associated with delamination growth. Next, a critical value of G for delamination onset was determined. It was then used to predict the onset of delamination in $[+45_n/-45_n/0_n/90_n]_s$ (n=1,2,3) laminates. A delamination resistance curve (R-curve) was developed to characterize the observed stable delamination growth during quasi-static loading. Finally, a power law correlation between G and delamination growth rates in fatigue was established.

SYMBOLS

[A]	extensional stiffness matrix
A	delaminated area
A*	area of interface containing a delamination
a	strip delamination size
Δa	incremental strip delamination size
$\frac{da}{dN}$	delamination growth rate in fatigue
[B]	coupling stiffness matrix
b	half-width of laminate cross section
C,β	empirically determined coefficients
[D]	bending stiffness matrix

E axial stiffness of a partially delaminated laminate

E_{LAM} axial laminate stiffness calculated from laminated plate theory

E^* axial stiffness of a laminate completely delaminated along one or more interfaces

E_i axial stiffness of the i^{th} sublaminate formed by a delamination

E_o initial tangent modulus of an undamaged laminate

E_{11}, E_{22}, E_{33} lamina moduli

$\frac{dE}{dA}$ rate of stiffness change with delamination area

$\frac{dE}{dN}$ rate of stiffness change with fatigue cycles

G_{11}, G_{12}, G_{13} lamina shear moduli

G strain energy release rate associated with delamination growth

G_I, G_{II}, G_{III} strain energy release rate components due to opening, in-plane shear, and out of plane shear fracture modes

G_{FEM} values of G_I, G_{II}, G_{III} calculated from finite element analysis

G_c critical strain energy release rate for delamination onset

G_R delamination resistance

G_{max} maximum strain energy release rate in constant strain amplitude fatigue test

h	ply thickness
K	saturation spacing of cracks in 90° plies
ℓ	gage length used to measure axial displacements
N	number of fatigue cycles
n	number of plies in a laminate
t	laminate thickness
t_i	thickness of i^{th} sublaminate formed by delamination
u,v,w	displacements in x,y,z directions
U,V,W	displacement functions in x,y,z directions
v	material volume
$\frac{du}{dA}$	rate of strain energy released as flaw extends
$\frac{dw}{dA}$	rate of work done by applied load as flaw extends
x,y,z	cartesian coordinates
X,Y,Z	nodal forces in x,y,z directions
X_{11}	first element of the inverse extensional stiffness matrix (A_{ij}^{-1}) $(i,j = 1,2,3)$
ε	nominal axial strain
ε_o	uniform axial strain assumed in finite element analysis

ε_c nominal axial strain at onset of delamination

ε_{max} maximum cyclic strain level in fatigue

$\nu_{12}, \nu_{13}, \nu_{23}$ lamina Poisson's ratio

σ_x axial stress in a ply

σ_c remote axial stress applied at onset of delamination

σ_z interlaminar normal stress between plies

SPECIMENS AND APPARATUS

Unnotched $[\pm 30/\pm 30/90/\overline{90}]_s$, T300-5208 graphite-epoxy laminates were tested in tension. This laminate was designed to have relatively high tensile interlaminar normal stresses at the edges resulting in the formation of a delamination [5]. Figure 1(a) shows the delamination that developed along the edge.

The specimens were 254 mm (10 in.) long by 38 mm (1.5 in.) wide. These eleven-ply laminates had an average ply thickness of 0.14 mm (.0054 in.). Specimens were tested in a closed-loop hydraulic testing machine. The specimen length between the grips was 180 mm (7.0 in.).

Also shown in figure 1(a) is a pair of linear variable differential transducers (LVDT's), that were mounted on the specimen to measure displacements over a 102 mm (4.0 in.) gage length. To prevent slippage, a fast drying glue was applied to the central 5.6 mm (.22 in.) portion of the LVDT mounts where they touched the specimen. During "strain-controlled" loading, these LVDT's were used as the feedback device in the closed loop.

Dye-penetrant enhanced radiography was used to monitor delamination growth through the specimen width. Diiodobutane (DIB), a dye penetrant opaque to x-rays, was injected along the delaminated edge. The film was placed immediately behind the specimen. While still mounted in the test machine, specimens were exposed to x-rays generated for five seconds at 18 kV from a portable point-source unit positioned 386 mm (15.5 in.) away from the specimen. The radiographs showed the location of the delamination front (fig. 1(b)). The dark outline in the center of the picture is the "shadow" (x-ray image) of the LVDT rods used to measure displacements.

DAMAGE DEVELOPMENT

The same type of damage developed during both quasi-static tension and constant-amplitude, tension-tension fatigue. First, a few isolated cracks formed in the 90° plies. These were followed almost immediately by the formation of small delaminations along the edge, as seen in figure 2(a). When the delaminations formed, the number of 90°-ply cracks increased significantly along the delaminated length of the specimen. Most of the 90°-ply cracks, which appear as horizontal lines on the radiographs in figure 2, extended beyond the delamination front outlined in the x-ray photograph. Many of the ply-cracks immediately extended halfway across the specimen width. As loading continued, additional delaminations formed and joined with original delaminations. Delaminations grew much more rapidly along the length of the specimen than across the width (fig. 2(b)). Eventually, two delaminations, one on each side of the specimen, extended along the entire specimen length between the grips (fig. 2(c)), after which

the delaminations continued to grow across the width. Loading was terminated when the delamination front reached the shadow of the LVDT rods (fig. 2(d)).

To illustrate the location of damage through the thickness, a few acetate tape replicas of a delaminated edge were made [6]. Figure 3 shows photographs of two replicas and a portion of the delaminated edge. As shown in figure 3(a), ply cracks extended through the thickness of all three interior 90° plies. As shown in figure 3(b), delaminations formed and grew in $-30^{\circ}/90^{\circ}$ interfaces, typically shifting from one interface, through 90° ply cracks, to its symmetric $-30^{\circ}/90^{\circ}$ counterpart. However, delaminations did not shift interfaces at every 90° ply crack encountered. As shown in a photograph of the delaminated edge, figure 3(c), interface shifting did not occur in a regular pattern.

Besides formation of delaminations at the -30/90 interfaces and cracks in the 90° plies, an occasional angular crack formed in the innermost -30° ply. The replica of the edge in figure 4(a) shows two angular cracks in the innermost -30° plies originating at a 90° ply crack tip and creating delaminations in the +30/-30 interfaces. As shown in the radiograph in figure 4(b), the delaminations in the +30/-30 interfaces were small and triangular in shape. These +30/-30 delaminations often temporarily arrested initial -30/90 interface delamination growth along the length of the edge. However, -30/90 interface delaminations eventually joined up and grew, whereas isolated +30/-30 delaminations usually remained small.

STRESS ANALYSIS

Two approximate analyses were used to obtain quantitative predictions of the onset and growth of delaminations. The first was a quasi-three-dimensional stress analysis that yielded stress distributions and strain

energy release rates. The second was a simple rule of mixtures analysis that was used along with laminated plate theory to calculate stiffness loss and strain energy release rates.

Because delaminations form in unnotched laminates as a result of the interlaminar stresses that develop at the edge, a quasi-three-dimensional finite element analysis [7] was performed. The finite element analysis was used to calculate stress distributions in the $[\pm 30/\pm 30/90/\overline{90}]_s$ laminate for a unit axial nominal strain ($\varepsilon_o = 1$). Some details of the analysis are described in Appendix A.

Figure 5 shows that the through-thickness distribution of the interlaminar normal stress, σ_z, calculated at the edge is compressive in the outer 30° plies but reaches a relatively high tensile value at the -30/90 interface and throughout the 90° plies. Also shown in figure 5 is the approximate σ_z distribution through the thickness calculated from laminated plate theory and an assumed stress distribution across the width [8]. This plot also shows the highest tensile σ_z stresses to be at the -30/90 interface and within the 90° plies.

Figure 6 shows a distribution of σ_z across the specimen width, near the edge, at the -30/90 interface, as well as a distribution of the axial stress, σ_x, in the adjacent 90° ply. Both σ_z and σ_x have high tensile values at the edge.

These stress distributions showed reasonable correlation with the observed damage that developed. Indeed, examining σ_z and interlaminar shear stress distributions are helpful in identifying likely delamination sites. However, interlaminar stress distributions calculated from finite

element analyses were not useful for modeling damage growth quantitatively because the magnitude of calculated peak stresses at the edge varied with mesh size. Furthermore, linear elastic analysis suggests that the interlaminar stresses at ply interfaces can become singular at the edge [7]. This singular behavior would preclude the use of a failure criterion based on maximum interlaminar stress values. Therefore, an alternate approach, based upon strain energy release rates, was adopted to quantitatively describe the onset and growth of delaminations.

STIFFNESS LOSS

In many composite laminates, stiffness loss may reflect delamination growth. Furthermore, the rate of stiffness loss with delamination growth can be directly related to strain energy release rates. Therefore, analysis and experiments were performed to correlate laminate stiffness and delamination size.

Rule of Mixtures Analysis

To analyze stiffness loss due to delamination, a simple rule of mixtures analyses, along with laminated plate theory, was used. First, the stiffness (tangent modulus) of a balanced, symmetric composite laminate (fig. 7a) was calculated from laminate theory [9,10] as

$$E_{LAM} = \frac{1}{X_{11}\, t} \tag{1}$$

where X_{11} is the first element of the inverse extensional stiffness matrix, A_{ij}^{-1} $(i,j = 1,2,3)$, and t is the laminate thickness. Next,

assuming a complete delamination in one or more interfaces, and using the rule of mixtures assumption that the sublaminates formed undergo the same axial strain (but no longer have the same transverse strains), results in

$$E^* = \frac{\sum_{i=1}^{n} E_i t_i}{t} \tag{2}$$

where

E^* = stiffness of a laminate completely delaminated along one or more interfaces

E_i = the laminate stiffness of the i^{th} sublaminate formed by the delamination

t_i = the thickness of the i^{th} sublaminate

Although equation (2) represents a two-dimensional formulation, E^* will depend upon which interfaces delaminate. This, in turn, determines the stiffness, E_i, and thickness, t_i, of each new sublaminate. Hence, equation (2) is sensitive to the through-thickness location of the delamination. For the $[\pm 30/\pm 30/90/\overline{90}]_s$ laminate, assuming a delamination in both -30/90 interfaces (fig. 7b) equation (2) becomes

$$E^* = \frac{8E(\pm 30)_2 + 3E(90)_3}{11} \tag{3}$$

Finally an equation for the stiffness, E, of a partially delaminated specimen was developed using the rule of mixtures. Equal-sized delaminated

strips were assumed to exist at both edges of the laminate (fig. 7c). Then, by assuming the laminated and delaminated portions of the specimen act as independent components loaded in parallel, the rule of mixtures yields

$$E = \left(E^* - E_{LAM}\right) \frac{a}{b} + E_{LAM} \tag{4}$$

A more general form of equation (4) may be developed by assuming that the relationship between laminate stiffness loss and delamination size can be represented by

$$\frac{E - E_{LAM}}{E^* - E_{LAM}} = \frac{A}{A^*} \tag{5}$$

where

A = delaminated area

A^* = total interfacial area

Rearranging equation (5) yields

$$E = \left(E^* - E_{LAM}\right) \frac{A}{A^*} + E_{LAM} \tag{6}$$

Equation (4) is a special case of equation (6) where

$$\frac{a}{b} = \frac{A}{A^*}$$

Experiments

To verify the linear relationship between stiffness and delamination size implied by equations (4) and (6), four quasi-static tensile tests were conducted. The specimens were loaded in a strain controlled mode until a delamination formed. Then, the specimens were unloaded to ten percent of the peak nominal strain, DIB was placed on the specimen edges, and an x-ray photograph was taken. Next, the specimens were reloaded in increments of 250 μm/m above the previous maximum strain level. This procedure was repeated until the specimen was almost totally delaminated.

During each loading, output signals of the two LVDT's were averaged, and load deflection curves were plotted on an X-Y plotter. The initial linear portion of each plot was used to calculate laminate stiffness corresponding to the damage recorded in the previous x-ray photograph (fig. 8). Delaminated areas recorded on the photographs within the 102 mm (4 in.) gage length were measured with a planimeter. To minimize data reduction error, each delamination was traced three times and measured areas were averaged. Then, a strip delamination size, a, having equal area over the LVDT gage length as the measured delamination, was calculated (fig. 9).

Figure 10 shows a plot of normalized stiffness, E/E_o, as a function of normalized delamination size a/b. A least-squares regression line for the data indicated that $E^* = 0.742E_o$, where E_o is the initial tangent modulus measured. Hence, a total delamination in the $[\pm 30/\pm 30/90/\overline{90}]_s$ laminate would result in a 25.8 percent reduction in laminate stiffness. The data agreed with the linear rule of mixtures equation (4), normalized by E_{LAM}, where E^* was calculated from equation (3) and sublaminate stiffnesses were calculated using equation (1) (see appendix B) with material properties from reference [11].

Finally, equations (2) and (4) were used iteratively to calculate laminate stiffness for specimens having -30/90 interface delaminations and concurrent, although small, +30/-30 interface delaminations (see Appendix C). The contribution of 90^{o} ply cracks to laminate stiffness loss was also considered (see Appendix C). However, the net effect of both secondary mechanisms (+30/-30 delaminations and ply cracks) on stiffness loss was negligible for the $[\pm 30/\pm 30/90/\overline{90}]_s$ laminate.

STRAIN ENERGY RELEASE RATE

For an elastic body containing a planar flaw of area A, the strain energy release rate, G, is the difference between the rate of work done, dW/dA, and the rate at which elastic strain energy is stored, dU/dA, as the flaw area increases [12], i.e.,

$$G = \frac{dW}{dA} - \frac{dU}{dA} \tag{7}$$

Assuming that a nominal strain, ε, is sufficient to extend the flaw, the work term vanishes. Then, if U is expressed as a product of the strain-energy-density and volume of the body, V, substituting Hooke's law into equation (7) yields

$$G = -V \frac{\varepsilon^2}{2} \frac{dE}{dA} \tag{8}$$

where $\frac{dE}{dA}$ is the rate of stiffness change as the flaw extends.

In this study, the body was a tensile-loaded, unnotched composite laminate, containing edge delaminations. The strain energy release rate associated with the growth of edge delaminations can be calculated by assuming two strip delaminations (fig. 9) where

$$\begin{aligned} V &= 2b\,\ell\,t \\ A^* &= 2b\,\ell \\ A &= 2\,\ell\,a \\ dA &= 2\ell\,da \end{aligned} \tag{9}$$

Then, substituting equations (9) into equation (8) and differentiating equation (4) yields

$$G = \frac{\varepsilon^2 t}{2}\left(E_{LAM} - E^*\right) \tag{10}$$

Equation (10) may also be derived for an arbitrary-shaped delamination by substituting equation (6) into equation (8), differentiating, and noting that $V = A^*t$. Hence, as indicated in equation (10), the strain energy release rate associated with delamination growth is independent of the delamination size. The magnitude of G depends only on the laminate layup and location of the delaminated interface(s) (which determine E_{LAM} and E^*), the nominal strain, ε, and the laminate thickness, t.

Furthermore, the strain energy release rate (eq. (10)) may have contributions from any of the three components G_I, G_{II}, or G_{III}, corresponding to the opening, in-plane shear, and out-of-plane shear fracture modes. In addition, near the edge, G may deviate from the value predicted by

equation (10), which was developed using laminated plate theory and the rule of mixtures. Therefore, a virtual crack extension technique was used with the quasi-three-dimensional finite element analysis to calculate G_I, G_{II}, and G_{III} as a function of delamination size (see Appendix A). As shown in figure 11, the finite element analysis indicated that the total G, represented by G_I plus G_{II} (G_{III} was negligible), reached the value predicted from equation (10) once the delamination had grown a very small distance in from the edge.

Because G increased rapidly with "a" near the edge, a small delamination that formed (for whatever reason) at the edge would be expected to undergo rapid initial growth. This behavior was observed in the quasi-static tension tests used to generate stiffness data. As soon as a delamination was detected, the loading was stopped. The formation and growth of the delamination to some finite size appeared to be nearly instantaneous. Therefore, G calculated from equation (10) at the nominal strain where delamination was first detected was considered to be the critical value, G_c, required to form the delamination. This G_c was then used to predict the onset of delamination in other laminates.

DELAMINATION ONSET

To predict the onset of delamination in other laminates, several things were done. First, tension tests of $[\pm 30/\pm 30/90/\overline{90}]_s$ laminates were run to determine the nominal strain level, ε_c, at which delamination begins. Next, ε_c was used in equation (10) to predict a critical G_c for the onset of delamination. Then, G_c was used to predict the nominal strain at the onset of delamination in other laminates. A more detailed description of the procedure follows.

Critical G_c Determination

First, eighteen $[\pm 30/\pm 30/90/\overline{90}]_s$ graphite epoxy laminates were loaded monotonically in tension at a rate of 44.5 N/sec (10 lbs/sec) until a delamination was detected. The load level corresponding to delamination onset was recorded and the corresponding applied stress, σ_c, was calculated. Then, to determine the nominal strain at the onset of delamination, ε_c, σ_c was divided by E_{LAM}, calculated from laminated plate theory using the following elastic properties from reference [11]

$$E_{11} = 138 \text{ GPa } (20.0 \text{ Msi})$$

$$E_{22} = 15 \text{ GPa } (2.1 \text{ Msi})$$

$$G_{12} = 5.9 \text{ GPa } (0.85 \text{ Msi})$$

$$\nu_{12} = 0.21$$

The average ε_c value was 3470 μm/m. In addition, ε_c was determined from LVDT measurements on the four tests conducted to generate stiffness data. In each of these four tests, the load deflection plot was linear until the delamination formed. The average value of ε_c where the load-deflection curve deviated from linear for these four tests was also 3470 μm/m.

Next, ε_c was substituted into equation (10) to determine G_c. Stiffness E_{LAM} and E^* were calculated from equations (1) and (3), respectively, using elastic properties from reference [11]. The average laminate thickness, measured with micrometers, was 1.51 mm (0.0594 in.). A value of 137 J/m^2 (0.78 in-lbs/in^2) was calculated for the critical strain energy release rate.

Delamination Onset Prediction

To predict the onset of delamination in other laminates, equation (10) was inverted to yield

$$\varepsilon_c = \sqrt{\frac{2\,G_c}{t\left(E_{LAM} - E^*\right)}} \tag{11}$$

The critical G_c determined from $[\pm 30/\pm 30/90/\overline{90}]_s$ laminate data was used in equation (11) to predict the nominal strain at the onset of delamination in $[+45_n/-45_n/0_n/90_n]_s$ (n = 1,2,3) T300-5208 graphite-epoxy laminates having the same stacking sequence but different thicknesses. To evaluate E^*, delaminations were modeled along both 0/90 interfaces where high tensile σ_z stresses were anticipated [3] on the basis of the approximate analysis of reference [8]. Delaminations have been observed in the 0/90 interface of a $[\pm 45/0/90]_s$ laminate in reference [12]. Then, stiffnesses E_{LAM} and E^* were calculated from equations (1) and (2), respectively, using elastic properties from reference [11].

A ply thickness of 0.15 mm (0.0057 in.) was determined in reference [3] for the 8-ply (n = 1), 16-ply (n = 2), and 24-ply (n = 3) laminates. In figure (12), predictions of ε_c were compared to ε_c values calculated by dividing measured σ_c values from reference [3] by E_{LAM}. Because the data from reference [3] represents the average of only two or three tests for each stacking sequence, only preliminary conclusions can be drawn. Nevertheless, the good comparison indicates that G_c may be independent of the ply orientations that make up the delaminating interface. For example, G_c may be the same for delamination onset in the -30/90 interfaces of

$[\pm 30/\pm 30/90/\overline{90}]_s$ laminates and for delamination onset in the 0/90 interfaces of the $[+45_n/-45_n/0_n/90_n]_s$ (n = 1,2,3) laminates. In fact, equation (11) indicates that the dependence of ε_c on stacking sequence and the ply orientations that make up the delaminating interface is accounted for in the $(E_{LAM} - E^*)$ term.

In addition, both equation (11) and the data indicate that delaminations will form at a lower nominal strain in thicker laminates of identical stacking sequences. According to reference [4] interlaminar stress distributions calculated from elastic analysis will be identical for all $[+45_n/-45_n/0_n/90_n]_s$ laminates subjected to the same applied stress. Therefore, the authors concluded that a failure criterion, if based on critical interlaminar stresses, would not predict the thickness dependence of delamination onset. Hence, the strain energy release rate appears to be the most useful parameter for quantitatively predicing the onset of delamination after the delamination-prone interface(s) have been identified from a stress analysis.

DELAMINATION GROWTH

Quasi-Static Tension

Edge delamination has been observed to be a stable fracture process in laminates subjected to tension loading [1,5,14]. Hence, the applied load must be increased to force the delamination to grow. Tension tests on the $[\pm 30/\pm 30/90/\overline{90}]_s$ laminates confirmed this observation. Unstable growth of the delamination through the width did not occur before the laminate failed (fractured into two pieces). In the four quasi-static tests conducted to generate stiffness data, delaminations did not grow after the mean applied load exceeded 13,350 N (3000 lbs). The four laminates eventually

failed at a mean load of 20,000 N (4500 lbs). Therefore, the $[\pm 30/\pm 30/90/\overline{90}]_s$ laminate is well suited to studying stable delamination growth.

The stable growth of flaws can be characterized using the crack growth resistance curve (R-curve) concept of fracture mechanics [15]. Therefore, a delamination resistance curve was constructed. Strain energy release rates, G, were calculated from equation (10). Because G does not depend on delamination size, it appears as a horizontal line in figure 13. The three horizontal lines shown are G values calculated for a single specimen at three successive nominal strain levels. In addition, the delamination resistance, G_R, was calculated using the maximum nominal strain in equation (10). However, G_R was plotted as a point corresponding to the size (see fig. 9) of the delamination created by the nominal strain. As shown in figure 13, the curve formed by all such points, generated during the four $[\pm 30/\pm 30/90/\overline{90}]_s$ quasi-static tension tests, constitutes the delamination growth resistance curve (R-curve) for the graphite epoxy specimens tested. The critical G_c used in the previous section to predict the onset of delamination represents the first value of G_R, i.e., the first point on the R-curve. Hence, the R-curve characterizes the laminates resistance to delamination growth under tensile loading.

If the R-curve is independent of the ply orientations that make up the delaminated interface, like G_c appears to be (see previous section), then equation (10) and the R-curve can be used to predict the growth of delaminations under quasi-static tension in other laminates. As the loading is increased, G can be calculated from equation (10) and

compared with the R-curve to predict delamination size. Hence, delamination size as a function of applied load could be predicted for other laminates.

Fatigue

Experiments

Constant amplitude, tension-tension, strain-controlled fatigue tests of $[\pm 30/\pm 30/90/\overline{90}]_s$ graphite epoxy specimens were conducted at a frequency of 10 Hertz and a strain ratio of 0.2. Specimens were loaded slowly in tension until a small delamination appeared. Laminate stiffness was measured during this initial loading. Then, the specimen was unloaded and delamination size was recorded using DIB-enhanced x-ray photography. Next, the specimen was reloaded to the mean strain and the stiffness of the delaminated specimen was recorded. Then, constant-strain-amplitude cyclic loading was applied. The cyclic loading was interrupted at specified intervals to measure delamination size and static stiffness. Hence, a photographic record of delamination size and a record of static stiffness as a function of load cycles were accumulated. Cyclic loading was terminated when the delamination had grown across most of the specimen width and the front was obscured by the x-ray image of the LVDT rods (fig. 2(d)).

Delamination growth rate measurements

Figure 14 shows a typical plot of delamination size as a function of load cycles. A strip delamination size, a, was calculated from the delaminated area (fig. 9) measured from x-ray photographs using a planimeter. Three separate planimeter tracings of each delaminated area were performed to minimize data reduction error. As indicated in figure 14, once the delamination had grown over the entire length of the specimen edge, a constant growth

rate, da/dN, was eventually achieved. Table 1 lists the growth rates, da/dN, determined from least squares linear regression analysis of the data for each fatigue test.

Figure 15 shows a typical plot of static stiffness loss as a function of load cycles. This plot also became fairly linear once the delamination had grown away from the edge. Stiffness degradation rates, dE/dN, were calculated from least squares linear regression analysis of the data over the same cyclic range used to fit da/dN data. Because stiffness was found to be linearly related to delamination size, differentiating both sides of equation (4) with respect to number of cycles (N) allowed an alternate determination of delamination growth rates, da/dN, from measured stiffness degradation rates, dE/dN, i.e.,

$$\frac{da}{dN} = \left(\frac{b}{E^* - E_{LAM}}\right) \frac{dE}{dN} \quad . \tag{12}$$

Therefore, delamination growth rates for the edge delamination specimens could be estimated without measuring the delamination size directly (Table 1). Hence, the $[\pm 30/\pm 30/90/\overline{90}]_s$ specimens used in this investigation should be useful for generating baseline delamination growth data.

Data correlation with analysis

Four fatigue tests were conducted at each of three maximum cyclic strain levels. The maximum cyclic strain levels, ε_{max}, chosen were 3000, 3250, and 3500 μm/m. The maximum strain energy release rate, G_{max}, was calculated from equation (10) using ε_{max}. Therefore, a constant ε_{max} test was also a constant G_{max} test. The mean of the four delamination growth

rates, da/dN, was determined for each of the three G_{max} levels. A power curve of the form $\frac{da}{dN} = cG_{max}^{\beta}$ was fit to the three mean values of da/dN and the three values of G_{max} using a least squares routine. An excellent correlation was achieved for both delamination growth rate measurement techniques.

Figure 16 shows $\frac{da}{dN}$ as a function of G_{max} for growth rates estimated directly from measured delaminated areas. The growth rates for all four tests at each G_{max} level are shown along with the mean growth rate. Figure 17 compares the least-squares power law fits using direct area measurements and indirect stiffness estimates of delamination growth rates. Because both da/dN and G can be calculated without direct measurement of delamination size, the stiffness technique presents a relatively simple means of generating data to determine the dependence of empirical parameters c and β on differences in load history, frequency, temperature, etc.

With the parameters c and β determined, the power law might be applied to other laminates. The calculated strain energy release rates could be used with c and β measured from edge-delamination baseline tests to determine delamination growth rates.

CONCLUDING REMARKS

Methodology Summary

A methodology for analyzing the onset and growth of delaminations in composite materials was formulated based on findings in the current work and in the literature. The methodology is as follows.

First, a stress analysis of the particular material, configuration, and loading must be performed. The analysis should establish where

delaminations will be located. For unnotched laminates, the approximate analyses discussed in this paper [8,16] might be adequate. After the location is established, the delamination onset and growth can be characterized quantitatively using strain energy release rates. Such a characterization incorporates the influence of material volume. Furthermore, determination of the singular stress field at the delamination front is not required.

The current work indicates that a total strain energy release rate may be sufficient to characterize the onset and growth of edge delaminations in tensile-loaded coupons. More work is required to determine if this is true for other configurations and loadings. However, if strain energy release rates must be separated into G_I, G_{II}, and G_{III} components using a numerical analysis, then the dependence of these calculated components on grid size should be carefully checked and documented.

Immediate Results

A simple rule of mixtures analysis, using laminated plate theory, indicated that laminate stiffness was a linear function of delamination size. The analysis accurately predicted stiffness loss due to edge delaminations in $[\pm 30/\pm 30/90/\overline{90}]_s$ graphite epoxy laminates. The linear stiffness relationship was used to derive a closed-form equation for the strain energy release rate, G, associated with delamination growth in unnotched laminates. The simple G equation was used to predict delamination onset in $[+45_n/-45_n/0_n/90_n]_s$ (n = 1,2,3) laminates using a critical G_c determined from $[\pm 30/\pm 30/90/\overline{90}]_s$ laminates. Stable delamination growth in the $[\pm 30/\pm 30/90/\overline{90}]_s$ laminates was characterized

by developing a delamination resistance curve (R-curve). Delamination growth in $[\pm 30/\pm 30/90/\overline{90}]_s$ laminates in fatigue was characterized by developing a power law correlation between G and delamination growth rates.

Potential Applications

Preliminary predictions of delamination onset in $[+45_n/-45_n/0_n/90_n]_s$ laminates using a critical G_c determined from tests on $[\pm 30/\pm 30/90/\overline{90}]_s$ laminates indicated that G_c may be independent of the ply orientations that make up the delaminating interface. If this is true for stable delamination growth with increased tensile load and delamination growth in fatigue, then the delamination resistance curve (R-curve) and power law developed on $[\pm 30/\pm 30/90/\overline{90}]_s$ laminates can be used to predict delamination growth in other laminates.

APPENDIX A

FINITE ELEMENT ANALYSIS

Formulation

The quasi-three-dimensional finite element analysis was developed in reference [7]. A displacement field of the form

$$\begin{aligned} u &= \varepsilon_o x + U(y,z) \\ v &= V(y,z) \\ w &= W(y,z) \end{aligned} \tag{A1}$$

was assumed, where ε_o was a prescribed uniform axial strain. Eight-noded quadrilateral, isoparametric elements with three degrees of freedom per node were used to model a cross section along the specimen length (fig. 18). Only one quarter of the cross section was modeled due to symmetry conditions. Each ply was modeled with one element through its thickness except for the central 90° ply, which was modeled with one element through its half-thickness. The graphite epoxy unidirectional properties [11] used in the analysis were

$$\begin{aligned} E_{11} &= 138 \text{ GPa } (20.0 \text{ Msi}) \\ E_{22} &= E_{33} = 15 \text{ GPa } (2.1 \text{ Msi}) \\ G_{12} &= G_{13} = G_{23} = 5.9 \text{ GPa } (0.85 \text{ Msi}) \\ \nu_{12} &= \nu_{13} = \nu_{23} = 0.21 \end{aligned} \tag{A2}$$

APPENDIX A

Virtual Crack Extension Technique

Previously, a virtual crack extension technique has been applied to finite element analysis of delaminations [1,4]. In this technique, the work required to close the delamination, expressed in terms of nodal forces and displacements, is assumed to be equivalent to the strain energy released as the delamination extends due to a constant nominal strain. This technique greatly simplifies the computation of G_I, G_{II}, and G_{III} because knowledge of the singular stress field near the crack tip is not required.

Figure 19 illustrates the technique as it was used with the quasi-three-dimensional finite element analysis. First, the nodal forces were calculated for an initial delamination of size a. Then, the delamination was extended an amount Δa and the resulting nodal displacements at the same location were calculated. The expressions for G_I, G_{II}, and G_{III} in terms of nodal forces and displacements were

$$G_I = \frac{1}{2\Delta a}\left[\left(Z_b^1 + Z_b^2\right)\left(W_b - W_c\right) + Z_d^2\left(W_d - W_e\right)\right]$$

$$G_{II} = \frac{1}{2\Delta a}\left[\left(Y_b^1 + Y_b^2\right)\left(V_b - V_c\right) + Y_d^2\left(V_d - V_e\right)\right] \qquad \text{(A3)}$$

$$G_{III} = \frac{1}{2\Delta a}\left[\left(X_b^1 + X_b^2\right)\left(U_b - U_c\right) + X_d^2\left(U_d - U_c\right)\right]$$

where, for example, Z_b^1 represents the force in the z direction at node b calculated from element 1.

Figure 11 shows G_I and G_{II} as functions of delamination size. G_{III} was negligible for this case. Strain energy release rates, G_{FEM},

calculated using equations (A3), where normalized by the constant value predicted from equation (10). The total G, represented by G_I plus G_{II}, reached the value* predicted by equation (10) once the delamination had grown a very small distance in from the edge. Furthermore, the total G calculated was not sensitive to mesh refinement. However, the values of G_I and G_{II} calculated were sensitive to mesh refinement.

Figure 11 shows the nodal discretization used in the finite element analysis. Four different initial delamination sizes, a, were modeled. For each a, the delamination was grown in ten increments, Δa, equal to one tenth

---

*Because the finite element analysis models only one quarter of the laminate cross section due to symmetry, the analysis assumes four delaminations grow simultaneously, two on each side, located in the -30/90 interfaces. However, in the derivation of equation (10), only a single delamination was considered on either edge to be consistant with the physically observed behavior shown in figure 3(c) and illustrated in figure 20(a). Making the same assumptions as the finite element analysis would have yielded

$$V = 2b\ell t$$

$$A^* = 4b\ell$$

$$A = 4\ell a$$

$$dA = 4\ell\, da$$

which would result in $G = \frac{\varepsilon^2 t}{4}\left(E_{LAM} - E^*\right)$. Hence, the values calculated from the finite element analysis using equations (A3) were doubled to be consistent with equation (10) and the observed physical behavior.

of the initial delamination size. As a was increased, the mesh refinement changed accordingly. For the smallest delamination size, G_{II} continually increased as the delamination grew, but G_I was constant for all ten increments of growth. The ten values of G_I for the smallest a are represented by a horizontal line segment. For the next three delamination sizes, both G_I and G_{II} were constant for all ten increments of growth, but the ratios G_I/G_{II} changed. For the largest delamination size modeled, G_I and G_{II} were identical, both equal to one-half the total G. Hence, calculations of G_I and G_{II} varied with mesh size.

APPENDIX B

EFFECT OF COUPLING ON STIFFNESS LOSS

The stiffness of an arbitrary composite laminate may be calculated from laminate theory [9,10] as

$$E_{LAM} = \frac{1}{[A'_{11}]t} \tag{B1}$$

where

$$[A'] = [A]^{-1} + [A]^{-1}[B][D^*]^{-1}[B][A]^{-1}$$

$$[D^*] = [D] - [B][A]^{-1}[B] \ .$$

and [A], [B], [D] are the extensional, coupling, and bending stiffness matrices, respectively, defined in reference [9]. If the laminate is symmetric, the [B] matrix vanishes, and equation (B1) reduces to equation (1).

For an arbitrary laminate containing delaminations in one or more interfaces, equation (B1) may be used in equation (2) to calculate the stiffnesses, E_i, of the sublaminates that are formed. For the $[\pm 30/\pm 30/90/\overline{90}]_s$ laminate, with delaminations modeled in both -30/90 interfaces, equation (2) becomes equation (3)

$$E^* = \frac{8E_{(\pm 30)_2} + 3E_{(90)_3}}{11}$$

APPENDIX B

If the $(\pm 30)_2$ sublaminate stiffnesses are calculated using equation (B1) and material properties from reference [11], then $E^* = 0.69\ E_{LAM}$, which exceeds the value of E^* extrapolated from a least-squares regression line for the stiffness data. However, both -30/90 interfaces did not delaminate complete (fig. 3). As shown in figure 20(a), delaminations shifted from one -30/90 interface to another through various 90° ply cracks. Delaminations were believed to grow in this manner to reduce the effect of bending-extension coupling that would have been present had only one interface been cleanly delaminated or had both interfaces delaminated at the same time. Therefore, delaminations were modeled over both -30/90 interfaces (fig. 20(b)) but the bending-extension coupling in the $(\pm 30)_2$ sublaminates was neglected. Hence, the stiffness of each sublaminate was evaluated using equation (1). This resulted in $E^* = 0.743\ E_{LAM}$ which agreed with the value of E^* extrapolated from a least-squres regression line for the stiffness data (fig. 10).

In addition, stiffness loss for delaminations of various size was calculated from the finite element analysis. Concurrent strip delaminations were assumed in both -30/90 interfaces. Uniform axial extension was also assumed and, hence, bending-extension coupling was ignored. The stiffness corresponding to a particular delamination size was calculated using the technique outlined in reference [16]. Figure 21 shows the stiffness loss predicted by the linear rule of mixutes (R.O.M.) equation without coupling (E_i calculated from eq. (1)) and with coupling (E_i calculated from eq. (B1)). The finite element predictions agreed with the rule of mixtures equation that neglected bending-extension coupling. Hence, the finite element results also agreed with the data plotted in figure 10.

APPENDIX C

STIFFNESS CHANGE FROM SECONDARY MECHANISMS

Ninety Degree Ply Cracks

The spacings of 90° ply cracks in the laminated portion of partially delaminated $[\pm 30/\pm 30/90/\overline{90}]_s$ laminates were measured directly from enlarged x-ray photographs. The mean spacing is plotted in figure 22 as a function of delamination size (see fig. 9) for three quasi-static test specimens. As the delaminations grew, the crack spacings decreased to within values predicted by a simple one-dimensional model [6].

Near the 90° ply cracks, load was assumed to be transferred to the neighboring plies and then back into the 90° plies to form the next crack. The model predicted that 90° ply cracks would reach a characteristic saturation spacing, K, determined by the laminate stacking sequence, ply thickness, and ply stiffness, but independent of load history.

For the $[\pm 30/\pm 30/90/\overline{90}]_s$ laminate, the model predicted a saturation spacing of 0.838 mm (0.033 in.). For a $[\pm 30/\pm 30/90_3]$ sublaminate, representative of the delaminated portion of the $[\pm 30/\pm 30/90/\overline{90}]_s$ laminate, the model predicted a saturation spacing of 0.955 mm (0.0367 in.).

Stiffness change due to 90° ply cracking in the partially delaminated specimen was estimated by reducing the maximum axial stress in the 90° plies based on the density of cracks present. As shown in figure 23, the transverse stiffness of the 90° plies, E_{22}, was reduced by the percentage difference in the maximum axial stress, calculated from the one dimensional model, at the predicted crack spacing K and at one half the spacing K/2. This difference represents the reduction in load carried by the 90° ply once the saturation crack pattern has formed.

APPENDIX C

For the $[\pm 30/\pm 30/90/\overline{90}]_s$ laminate, a twelve percent reduction in the axial stress in the 90^o plies was predicted. Reducing, the transverse stiffness, E_{22}, of the 90^o plies by twelve percent resulted in a 0.7 percent reduction in $[\pm 30/\pm 30/90/\overline{90}]_s$ laminate stiffness. Similarly for the $[\pm 30/\pm 30/90_3]$ sublaminate, a 14 percent reduction in the axial stress in the 90^o plies was predicted. Reducing the transverse stiffness, E_{22}, of the 90^o plies by 14 percent resulted in a 2.2 percent reduction in the $[\pm 30/\pm 30/90_3]$ sublaminate stiffness.

Because the estimated contributions of 90^o ply cracks to stiffness reduction in the $[\pm 30/\pm 30/90/\overline{90}]_s$ delamination specimen were so small, they were neglected in calculating E^*. However, for other laminates and materials, ply cracking may have a greater effect on axial stiffness and other stiffness parameters [17,18].

+30/-30 delaminations

The largest +30/-30 interface delaminations, $\tilde{a}$, recorded during the four quasi-static tension tests were measured and tabulated in table 2. Only specimen E20 had a +30/-30 delamination of significant size. Also shown in table 2 are predicted stiffness values for the $[\pm 30/\pm 30/90/\overline{90}]_s$ laminate, containing both -30/90 and +30/-30 interface delaminations. The stiffness was predicted using equations (2) and (4) first for the +30/-30 delamination, and then for the -30/90 delamination. The stiffness predicted for specimen E20 was three percent less than the stiffness predicted assuming only -30/90 delamination. However, the data agreed best with the prediction that omitted the +30/-30 delamination. Hence, the effect of +30/-30 interface delaminations on measured $[\pm 30/\pm 30/90/\overline{90}]_s$ stiffness loss was neglected in calculating E^*.

REFERENCES

1. E. F. Rybicki, D. W. Schmueser and J. Fox, "An Energy Release Rate Approach for Stable Crack Growth in the Free-Edge Delamination Problem," J. Composite Materials, Vol. II (1977), p. 470.

2. G. L. Roderick, R. A. Everett, and J. H. Crews, Jr., "Debond Propagation in Composite-Reinforced Metals," Fatigue of Composite Materials, ASTM STP 569, American Society for Testing and Materials, 1975, pp. 295-306.

3. B. T. Rodini, Jr. and J. R. Eisenmann, An Analytical and Experimental Investigation of Edge Delamination in Composite Laminates, 4th Conf. on Fibrous Composites in Structural Design, San Diego, Calif., Nov. 14-17, 1978.

4. A. S. D. Wang, F. W. Crossman, and G. E. Law, "Interlaminar Failure in Epoxy-Based Composite Laminates," Proc. 29th Symp. Failure Modes in Composites, National Bureau of Standards, 1979.

5. L. M. Lackman and N. J. Pagano, "On the Prevention of Delamination in Composite Laminates," AIAA/ASME SAE 15th Structures, Structural Dynamics and Materials Conference, 1974, Paper No. 74-355.

6. K. L. Reifsnider, E. G. Henneke, and W. W. Stinchcomb, "Defect Property Relationships in Composite Materials, AFML-TR-76-81, Final Report, June 1979.

7. I. S. Raju and J. H. Crews, "Interlaminar Stress Singularities at a Straight Free Edge in Composite Laminates," NASA TM-81876, August 1980.

8. N. J. Pagano and R. B. Pipes, "Some Observations on the Interlaminar Strength of Composite Laminates," International Journal of Mechanical Science, Vol. 15 (1973), pp. 679-688.

9. R. M. Jones, Mechanics of Composite Materials, Scripta (1975).

10. T. K. O'Brien and K. L. Reifsnider, "Fatigue Damage: Stiffness/ Strength Comparisons for Composite Materials," Journal of Testing and Evaluation, Vol. 5, No. 5, 1977, pp. 384-393.

11. A. S. D. Wang and F. W. Crossman, "Some New Results on Edge Effect in Symmetric Composite Laminates," J. Composite Materials, Vol. II (1977), p. 92.

12. G. R. Irwin, "Fracture," Handbuch der Physik, Vol. 6 (1958), p. 551.

13. J. G. Bjeletich, F. W. Crossman, and W. T. Warren, "The Influence of Stacking Sequence on Failure Modes in Quasi-Isotropic Graphite Epoxy Laminates," Failure Modes in Composites - IV, AIME, 1979.

14. K. L. Reifsnider, E. G. Henneke, II, and W. W. Stinchcomb, "Delamination in Quasi-Isotropic Graphite-Epoxy Laminates," Composite Materials: Testing and Design (4th Conference), ASTM STP 617 (1977), p. 93.

15. Fracture Toughness Evaluation by R-Curve Methods, ASTM STP 527, American Society for Testing and Materials, Philadelphia, Pennsylvania, 1973.

16. T. K. O'Brien, "An Approximate Stress Analysis for Delamination Growth in Unnotched Composite Laminates," Proceedings of the Sixth Annual Mechanics of Composites Review, Dayton, Ohio, October, 1980.

17. A. L. Highsmith and K. L. Reifsnider, "The Effect of Tensile Fatigue Damage on Tensile, Compressive, and Bending Stiffness of Composite Laminates," Composites Technology Review, Vol. 2, No. 1, Winter 1980.

18. W. S. Johnson and G. J. Dvorak, "Mechanisms of Fatigue Damage in Boron/Aluminum Composites," Presented at ASTM Symposium on Damage in Composite Materials, Bal Harbour, Florida, November 10-14, 1980, (will appear in ASTM STP).

TABLE 1.- FATIGUE GROWTH RATE MEASUREMENTS

ε_{max} ($\mu m/m$)	G_{max} (J/m^2)	Spec. #	$\frac{da}{dN}$, $\frac{mm}{cycle}$ Area measure	$\frac{da}{dN}$, $\frac{mm}{cycle}$ Stiffness measure	$\frac{dE}{dN}$, $\frac{P_a}{cycle}$	Cycle range of linear fit (cycles $\times 10^3$)
3000	102	C20	26.0	22.3	-17.7	45 - 120
		F18	19.5	29.0	-22.9	40 - 120
		F24	24.5	27.0	-21.3	25 - 80
		C10	28.3	30.2	-23.8	40 - 115
		MEAN	24.6	27.1		
3250	119	A7	41.8	----	-----	40 - 80
		F3	63.9	64.2	-50.7	14 - 50
		E4	23.3	51.2	-40.3	40 - 70
		C16	23.6	25.4	-20.1	40 - 120
		MEAN	38.2	46.9		
3500	138	D2	52.6	106.2	-83.8	30 - 60
		B13	87.1	119.7	-94.5	16 - 40
		D22	64.6	39.7	-31.3	20 - 60
		B21	47.9	46.6	-36.7	28 - 75
		MEAN	63.0	78.0		

TABLE 2.- EFFECT OF +30/-30 DELAMINATION ON STIFFNESS PREDICTION

Specimen #	-30/90	+30/-30	E/E_{LAM} prediction		E/E_o measured
	$\frac{a}{b}$	$\frac{\tilde{a}}{b}$	With $\tilde{a}$	Without $\tilde{a}$	
F9	0.848	0.009	0.778	0.780	0.782
E20	.803	.109	.768	.792	.806
C18	.812	.004	.790	.790	.798
D6	.773	.004	.800	.800	.787

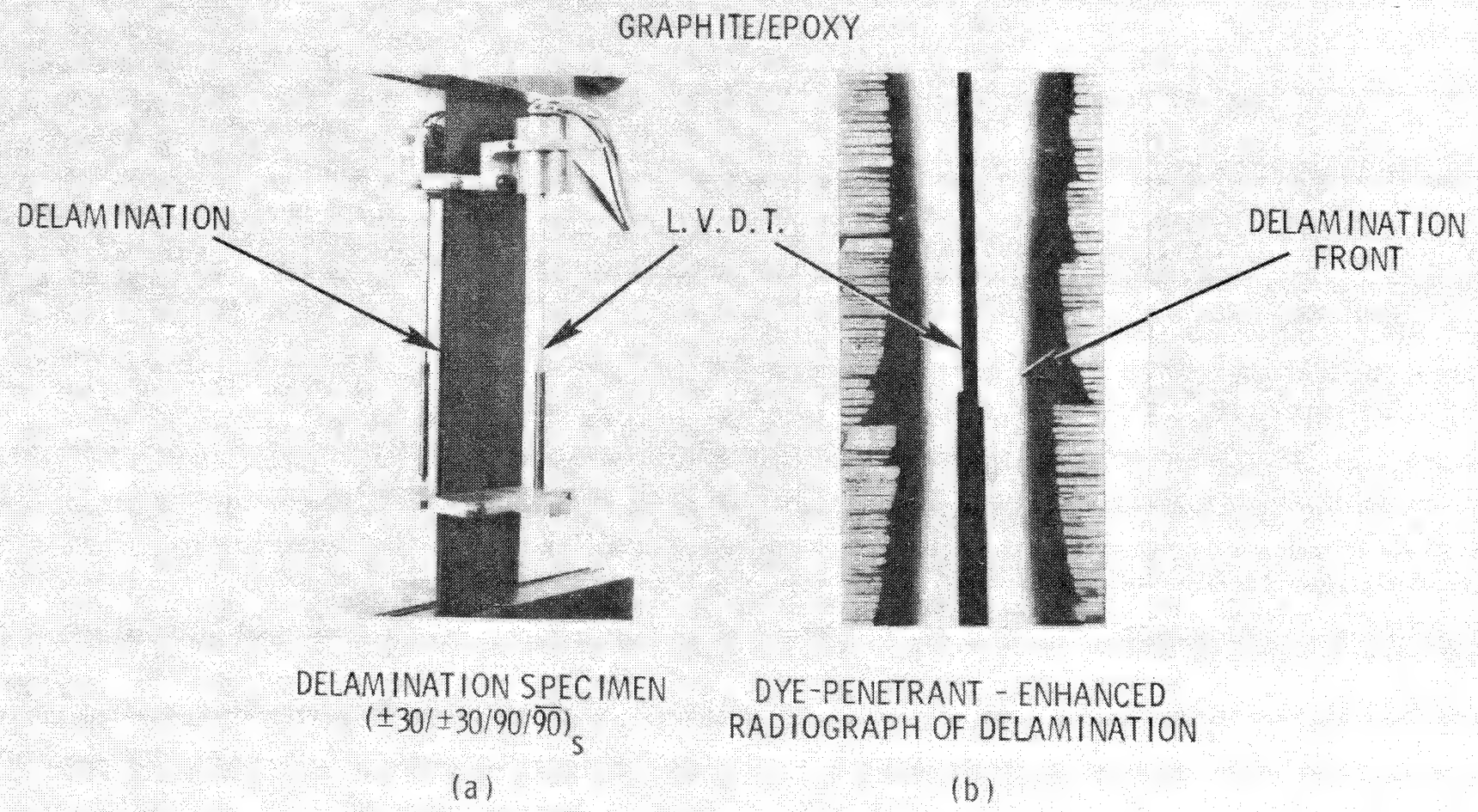

Figure 1.- Typical instrumented test specimen and dye-penetrant enhanced radiograph.

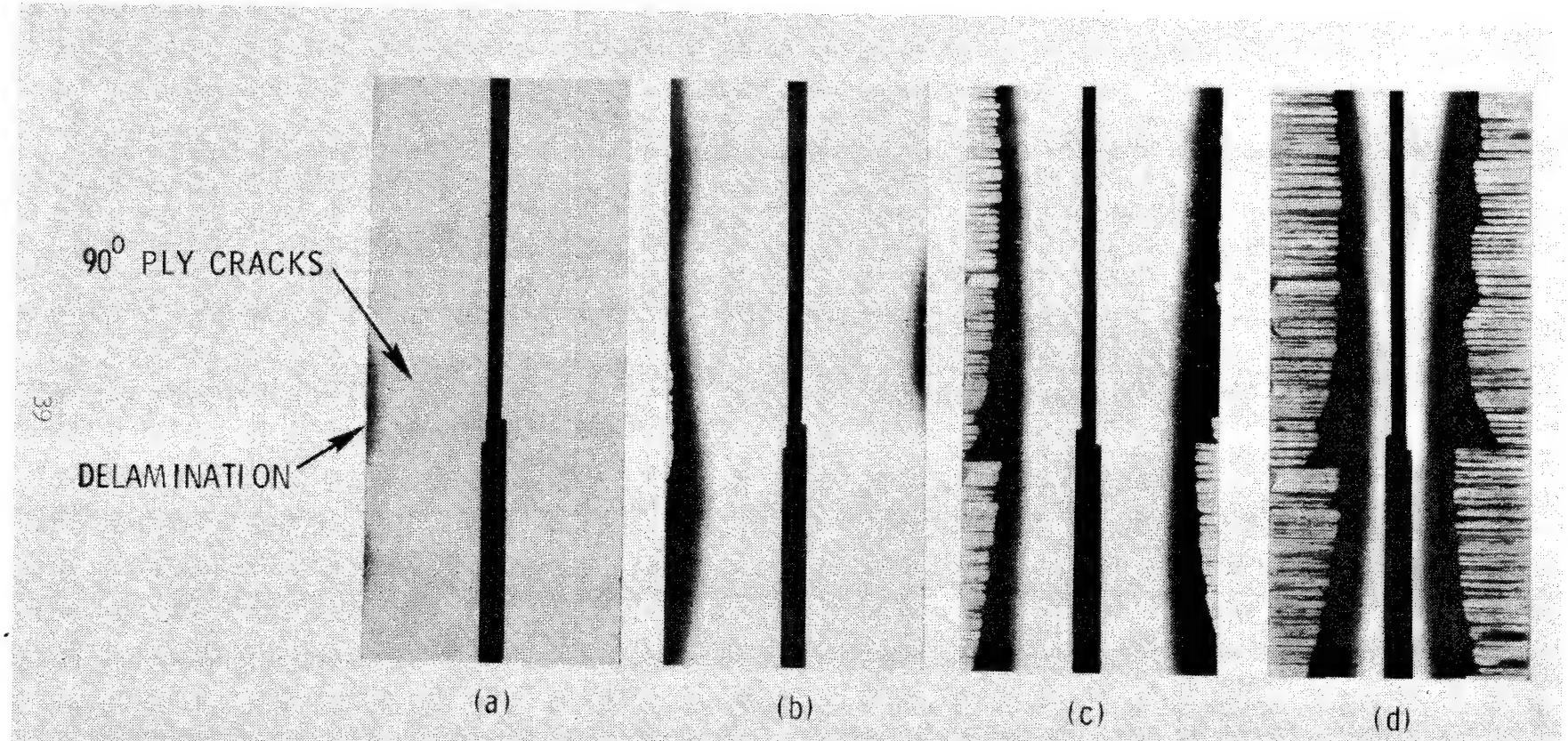

Figure 2.- Radiographs showing damage growth through the width of $[\pm 30/\pm 30/90/\overline{90}]_s$ laminates.

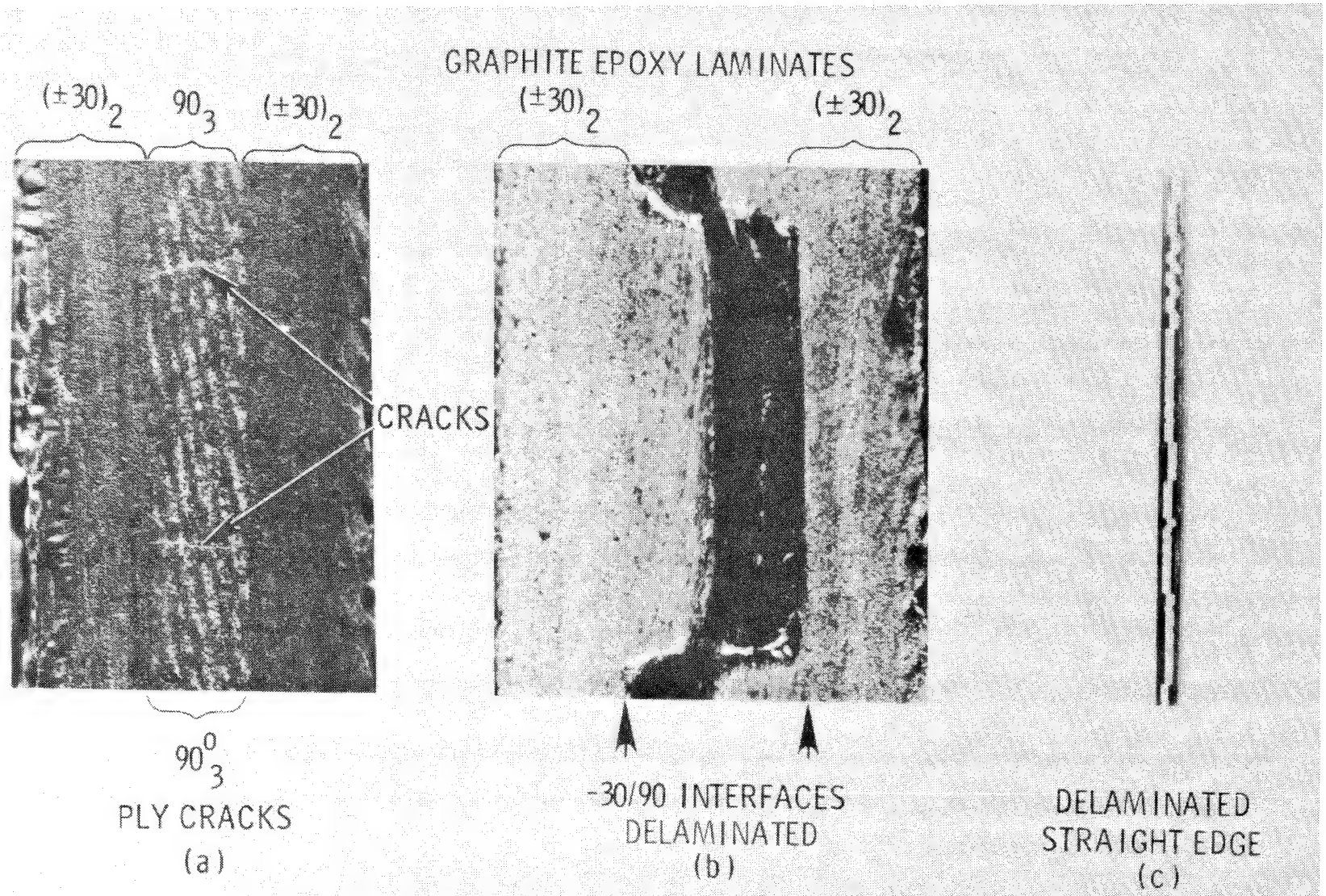

Figure 3.- Damage location through the thickness of $[\pm 30/\pm 30/90/\overline{90}]_s$ laminates.

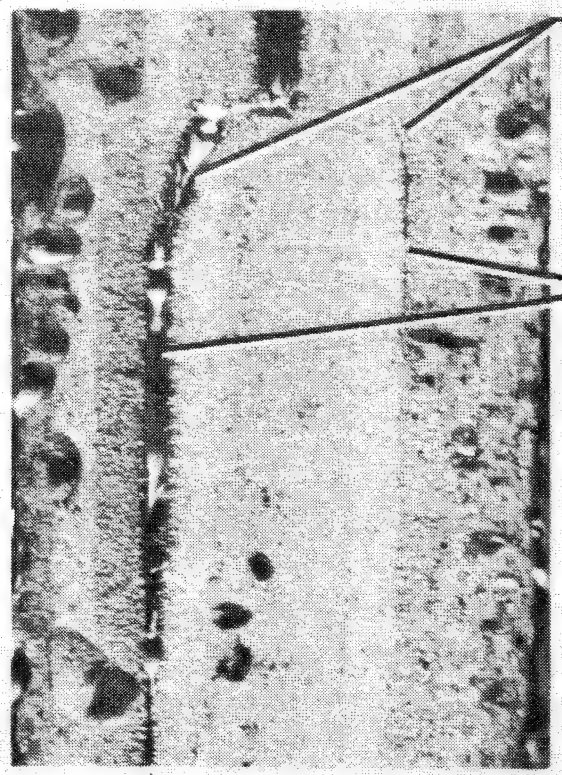

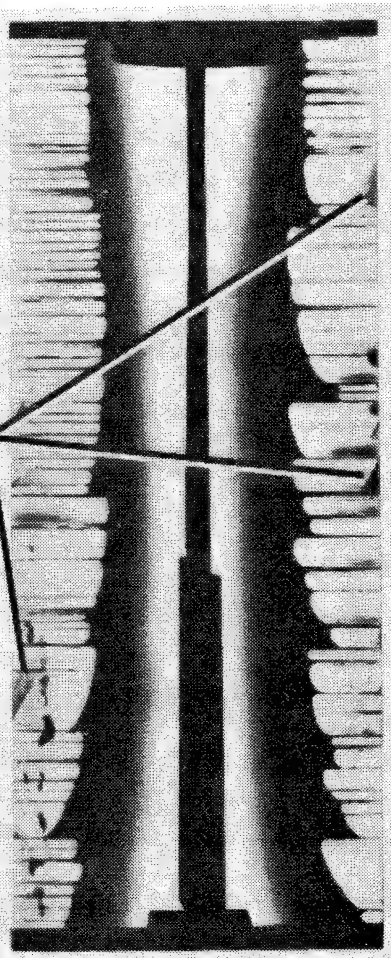

Figure 4.- Delaminations in +30/-30 interfaces.

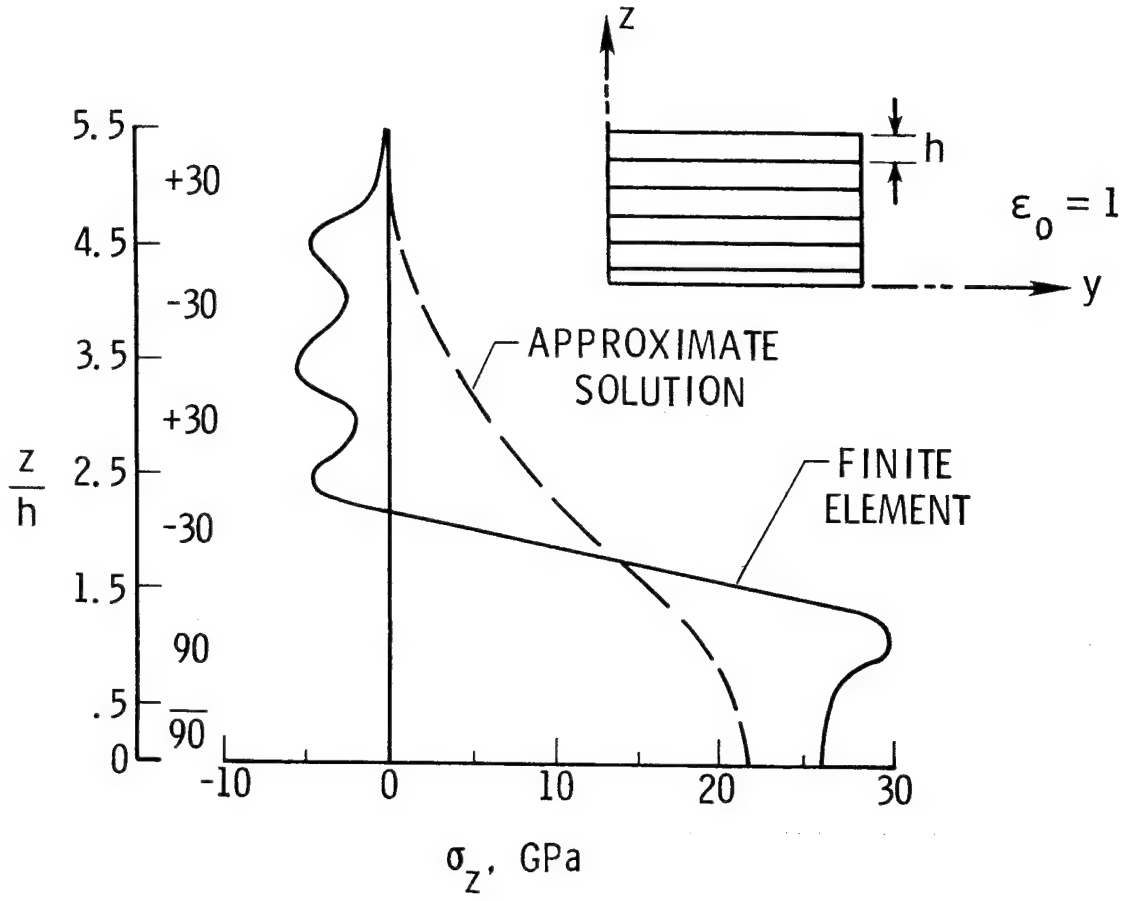

Figure 5.- Through-thickness σ_z distribution at edge of $[\pm 30/\pm 30/90/\overline{90}]_s$ laminate.

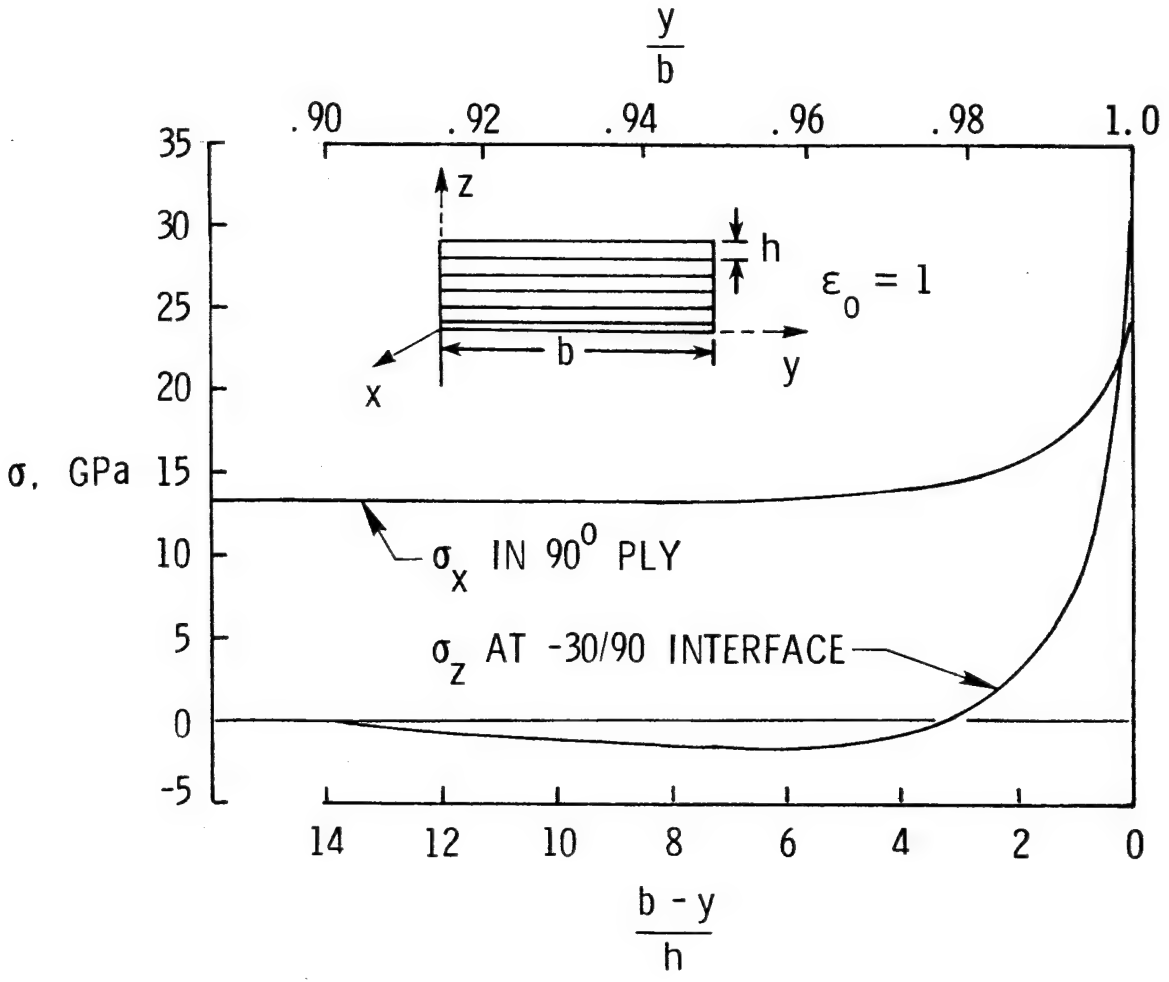

Figure 6.- Through-width distributions of σ_x and σ_z near the edge.

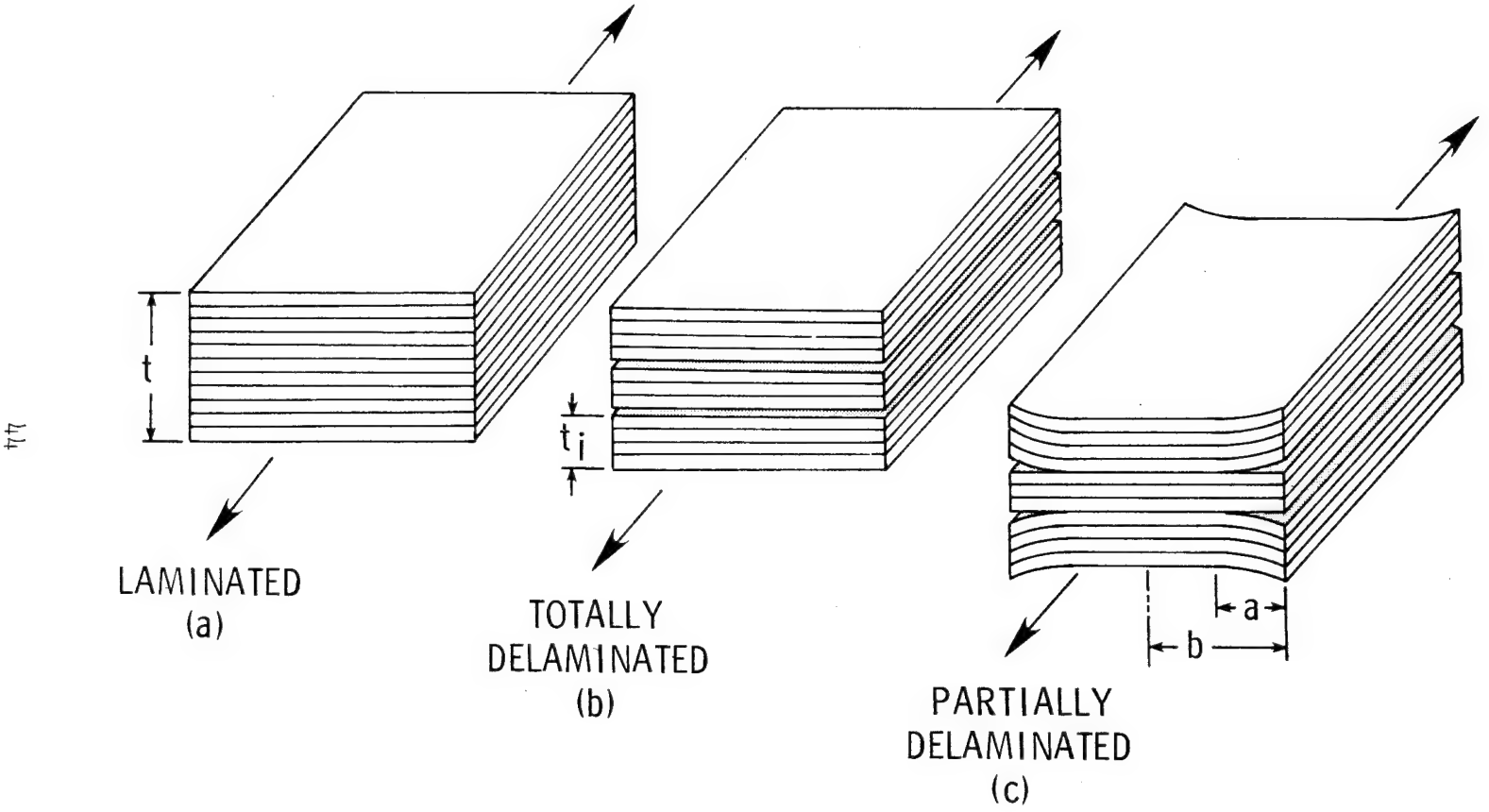

Figure 7.- Rule of mixtures analysis of stiffness loss.

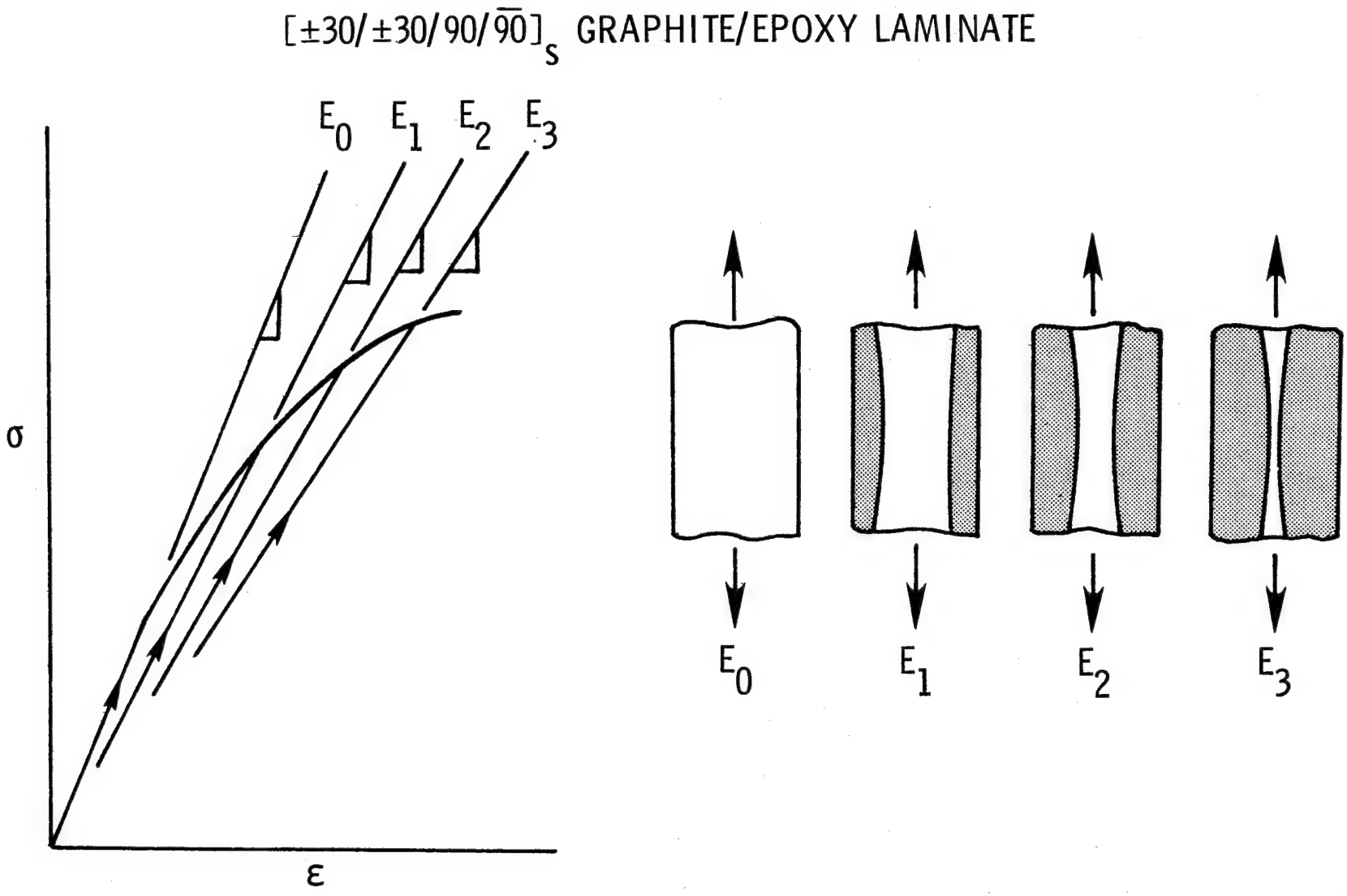

Figure 8.- Delamination size and stiffness data accumulation during quasi-static loading.

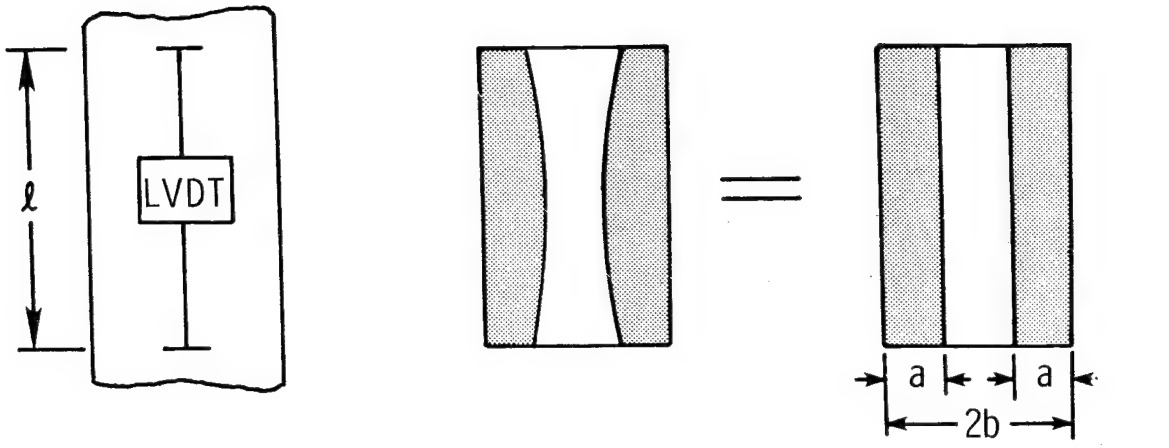

Figure 9.- Illustration of strip delamination approximation.

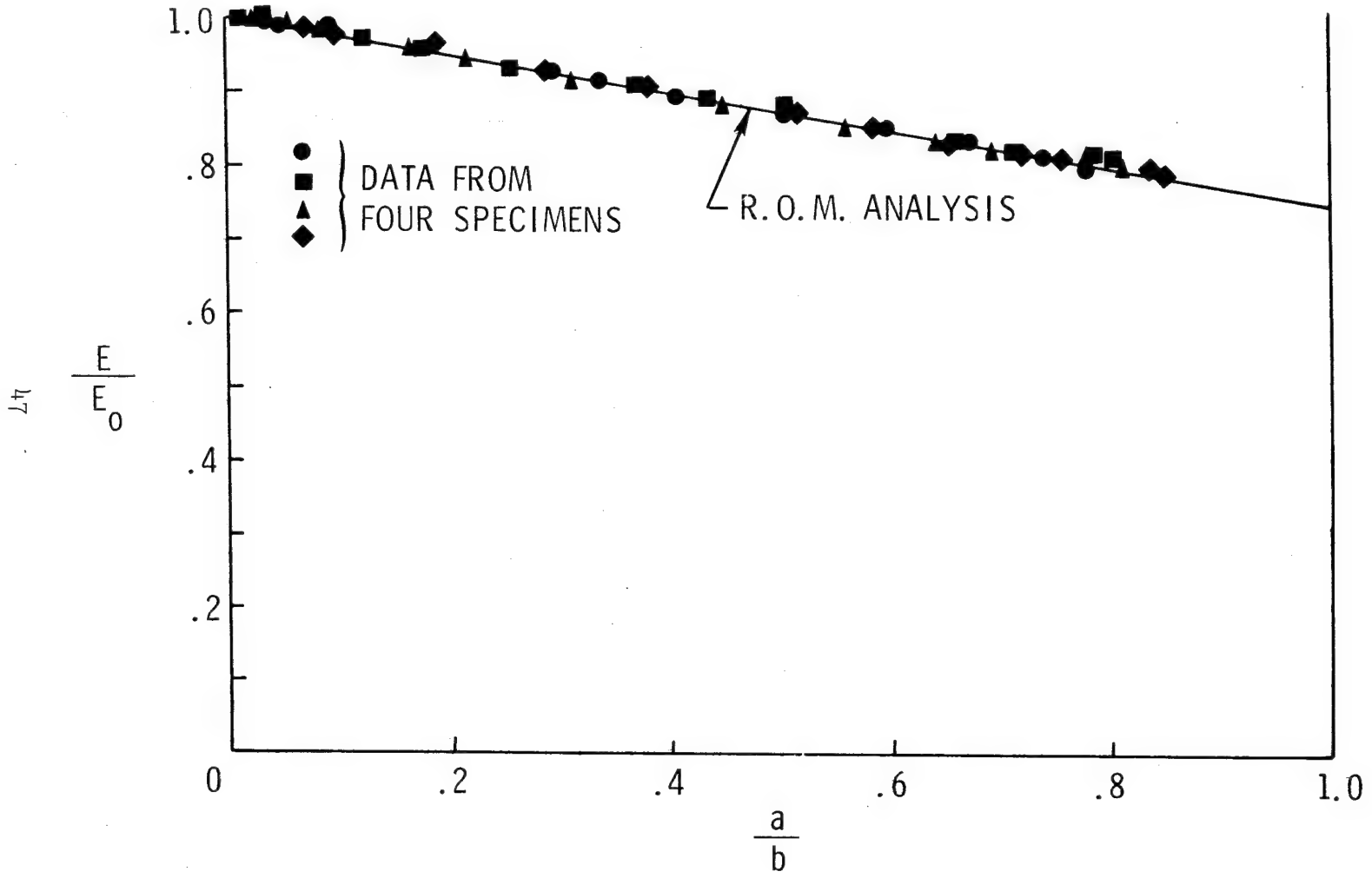

Figure 10.- Stiffness as a function of delamination size.

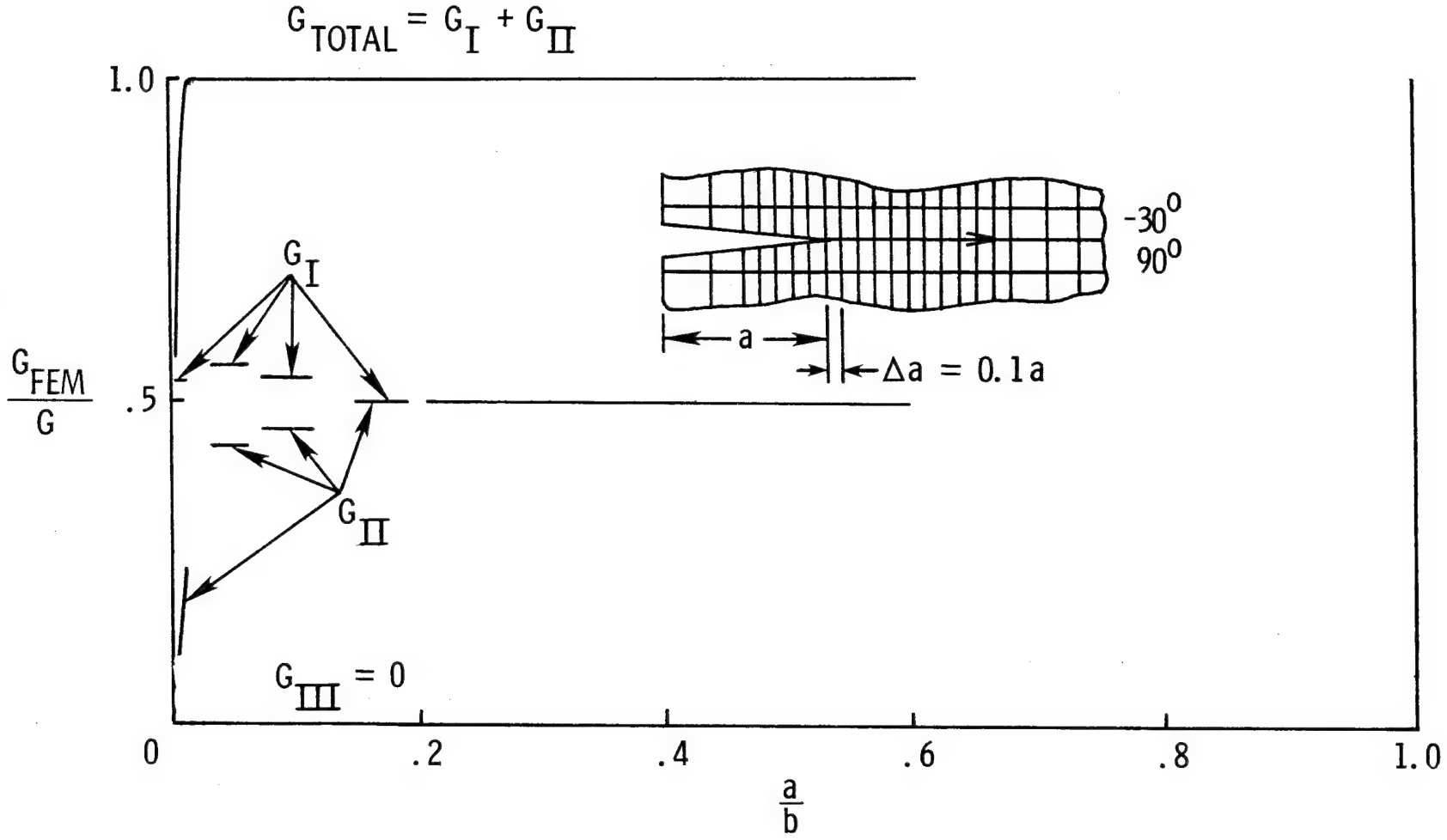

Figure 11.- Strain energy release rate components from finite element analysis as a function of delamination size.

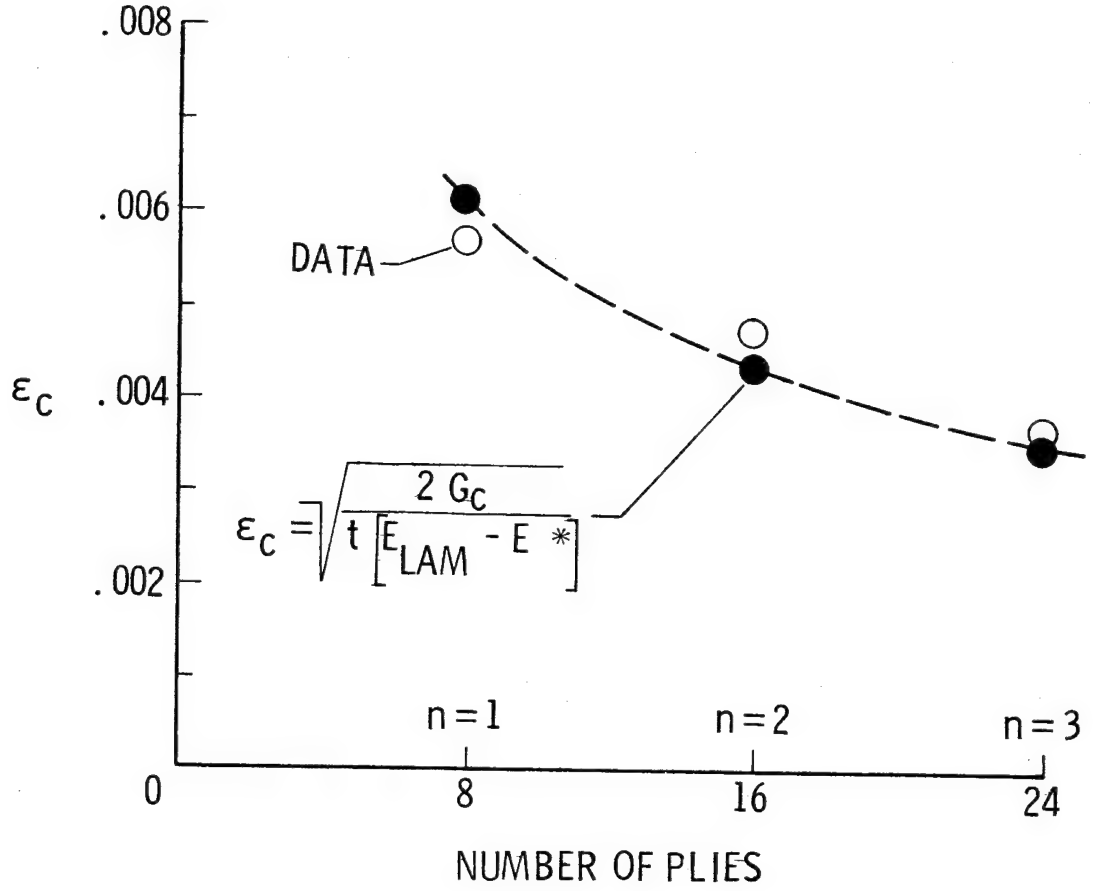

Figure 12.- Edge delamination onset prediction compared with $[+45_n/-45_n/0_n/90_n]_s$ (n = 1,2,3) data.

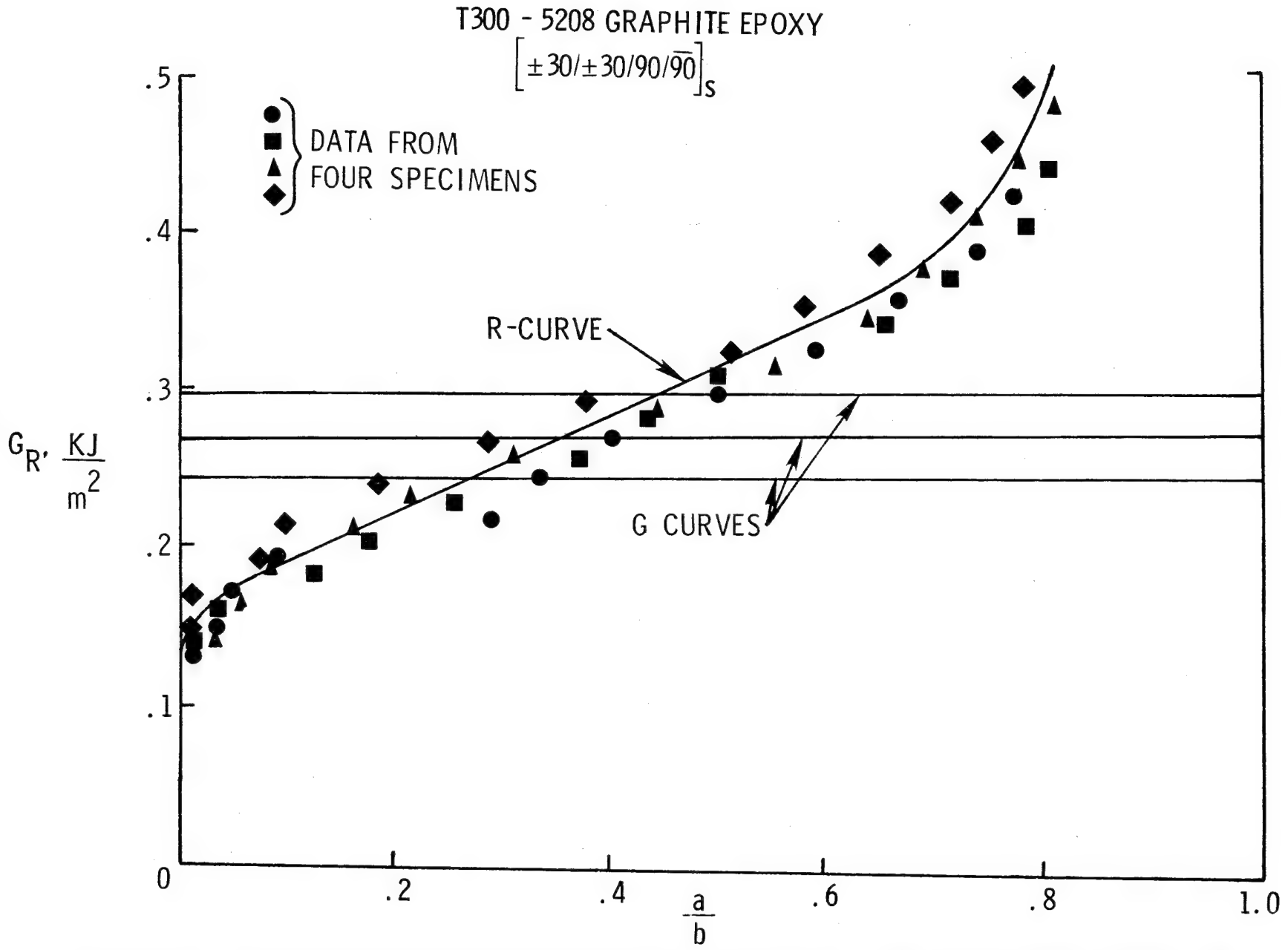

Figure 13.- Delamination resistance curve (R-curve) for $[\pm 30/\pm 30/90/\overline{90}]_s$ T300-5208 graphite-epoxy laminates.

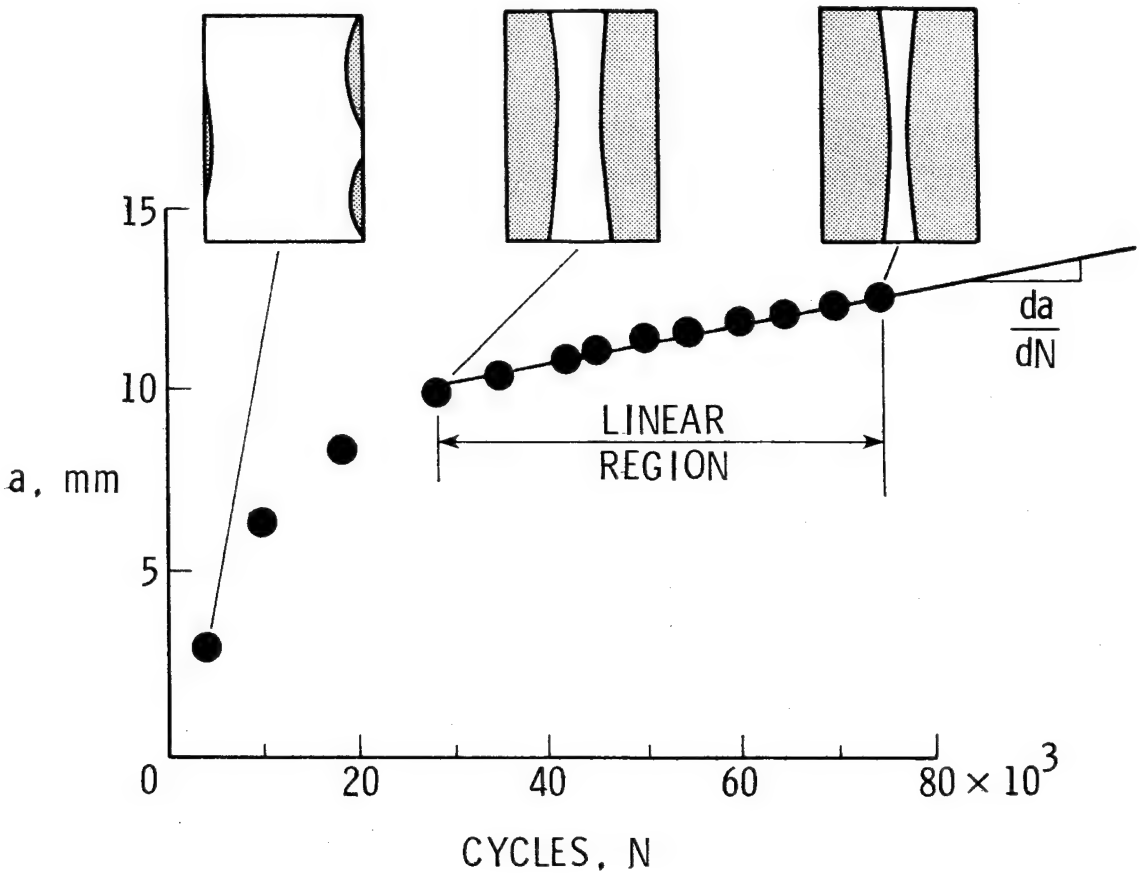

Figure 14.- Typical plot of delamination size as a function of load cycles.

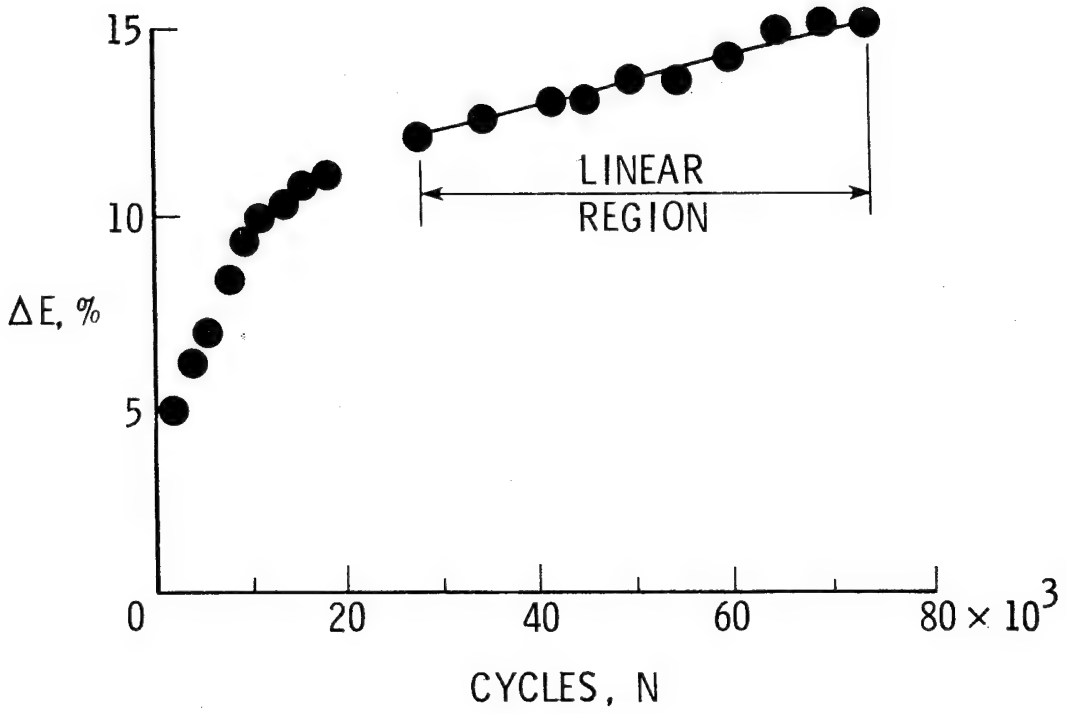

Figure 15.- Typical plot of static stiffness loss as a function of load cycles.

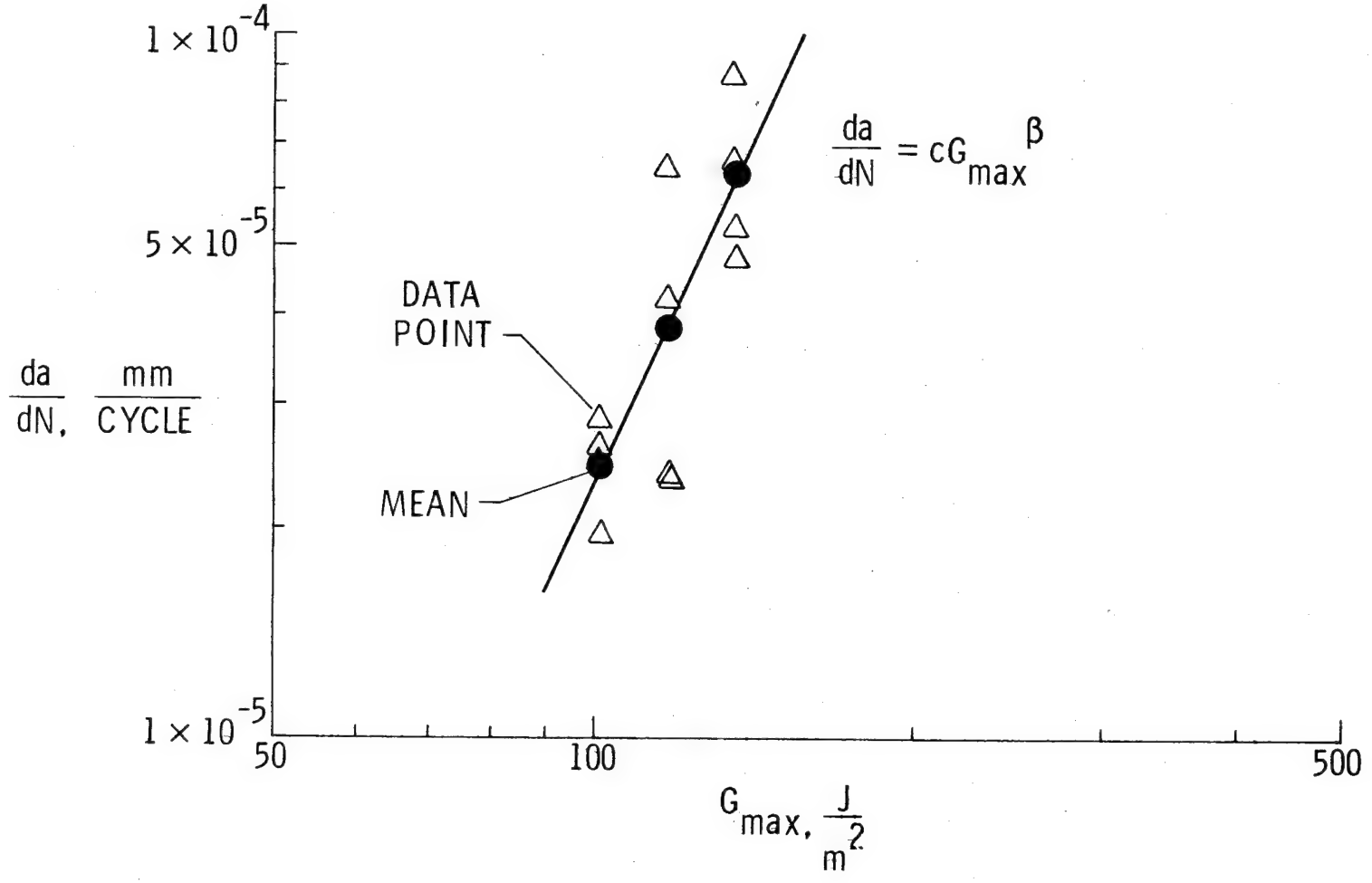

Figure 16.- Power law curve fit for $\frac{da}{dN}$ as a function of G_{max}.

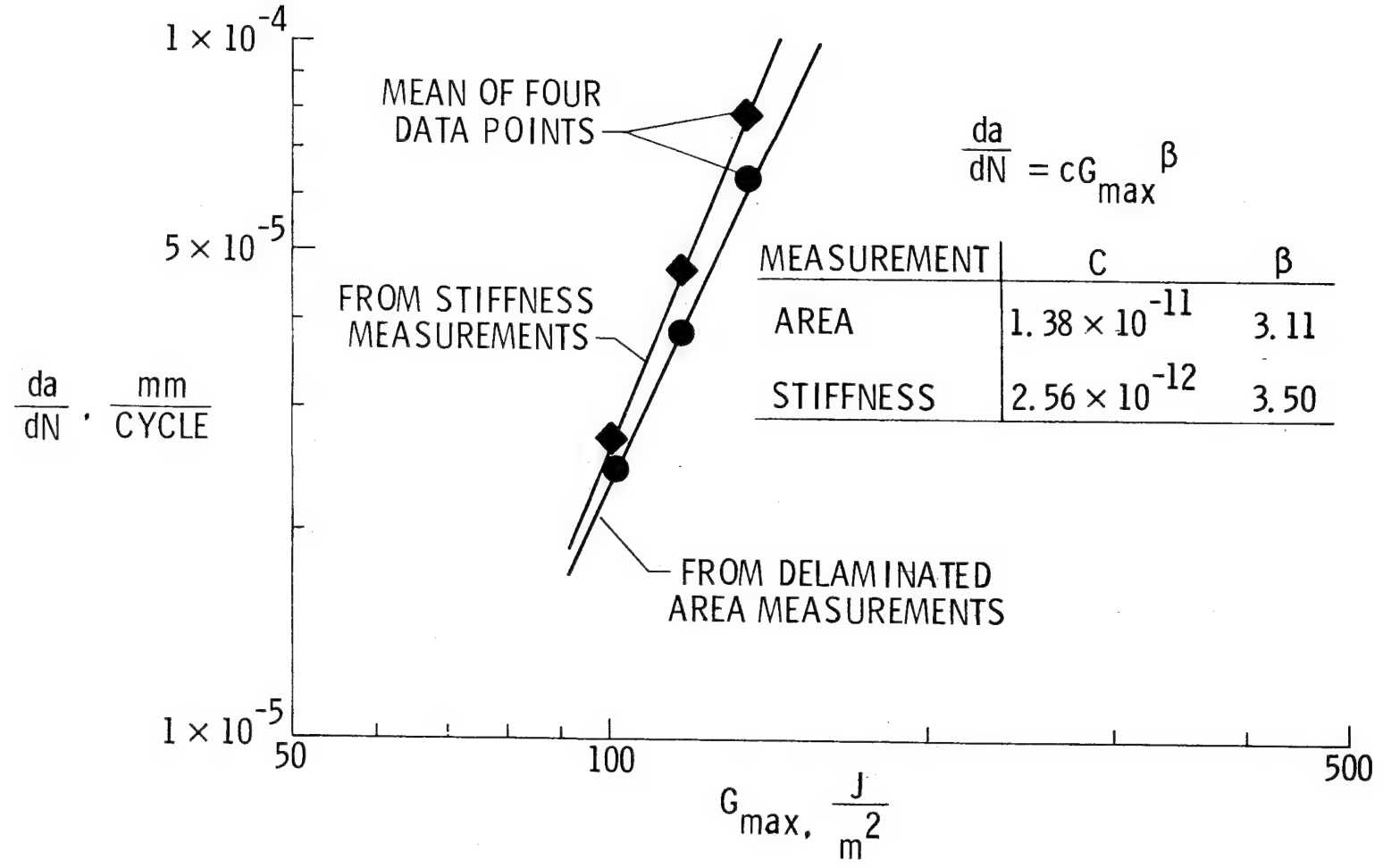

Figure 17.- Effect of delamination measurement method on power law curve fit.

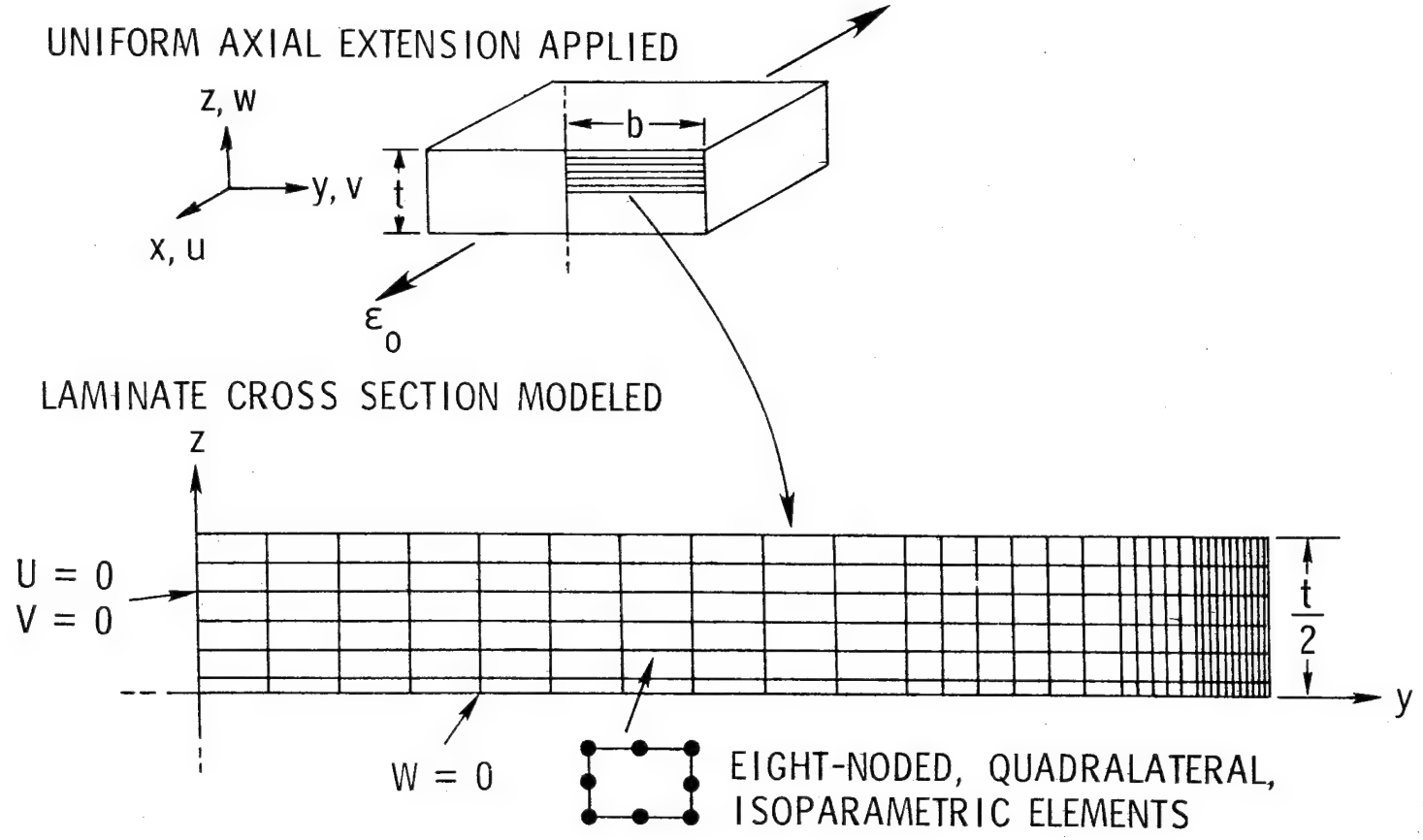

Figure 18.- Finite element discretization of specimen cross section.

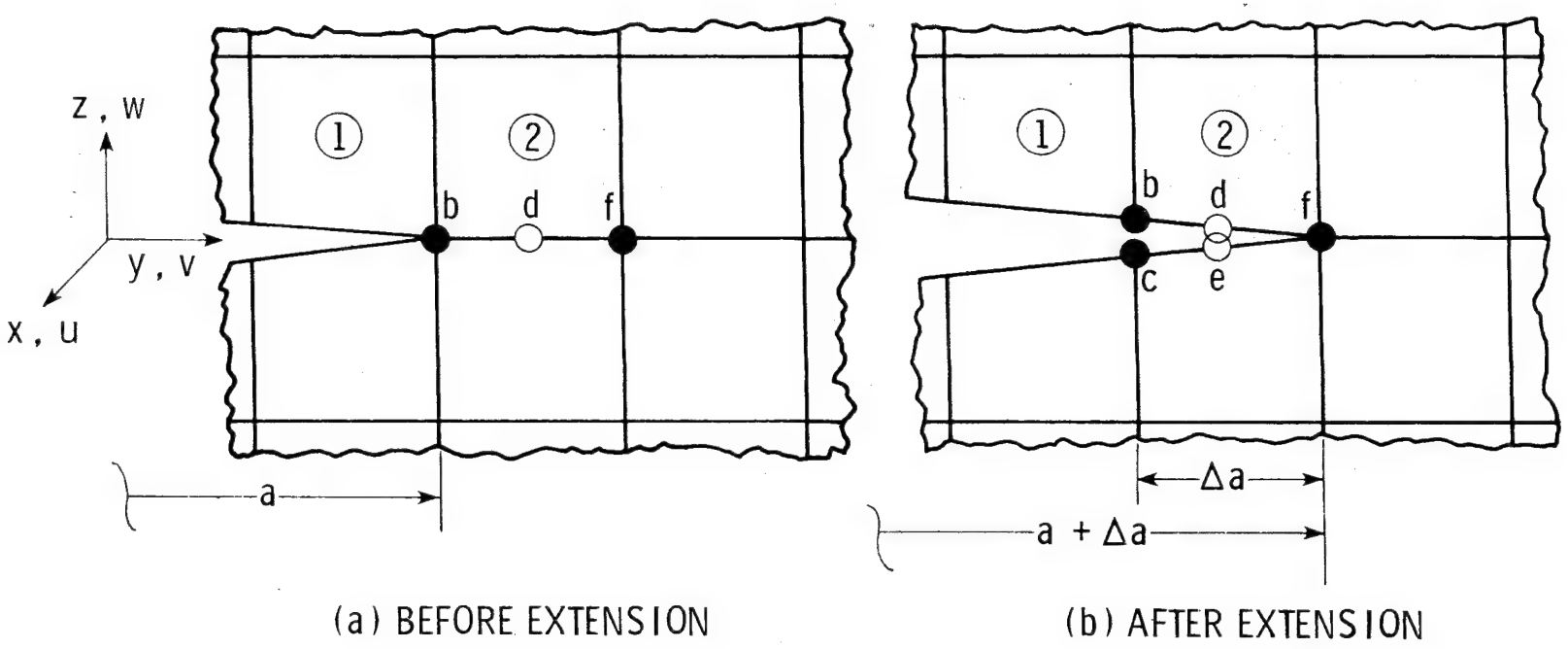

Figure 19.- Virtual crack extension technique used to calculate strain energy release rates.

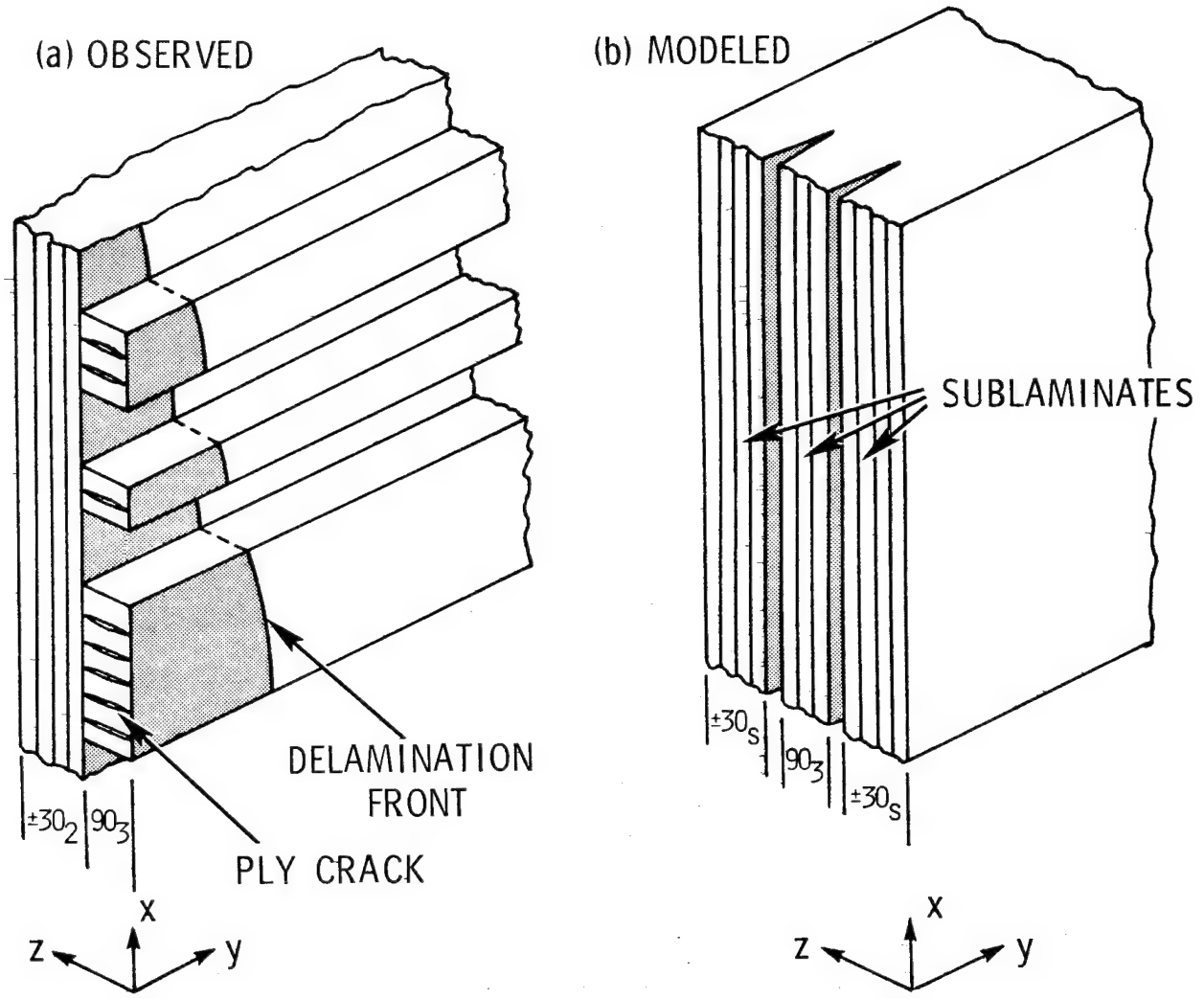

Figure 20.- Approximate model of observed damage.

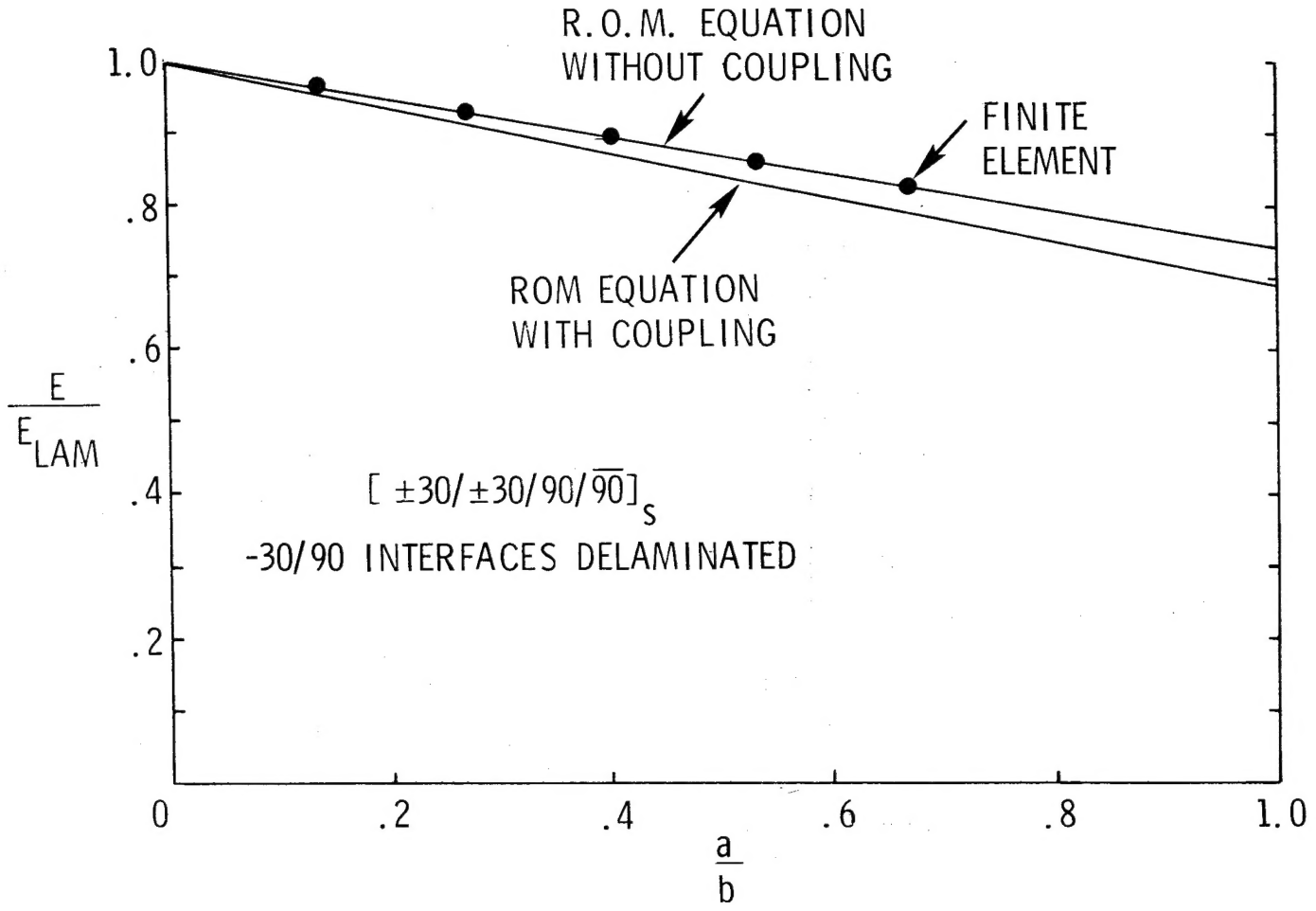

Figure 21.- Effect of coupling on stiffness loss prediction.

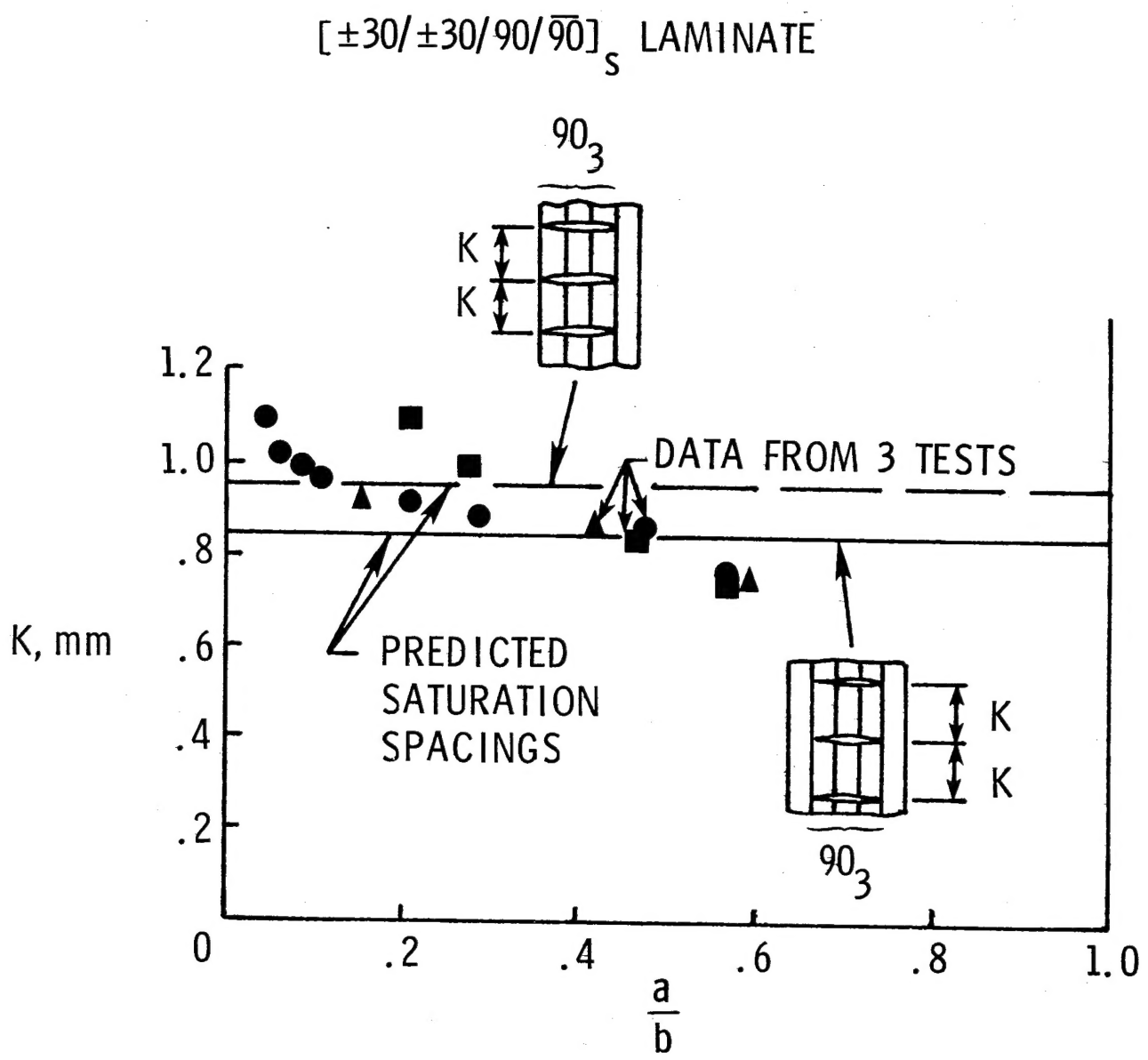

Figure 22.- Ninety degree ply crack spacing as a function of delamination size.

$[\pm 30/\pm 30/90/\overline{90}]_s$ LAMINATE

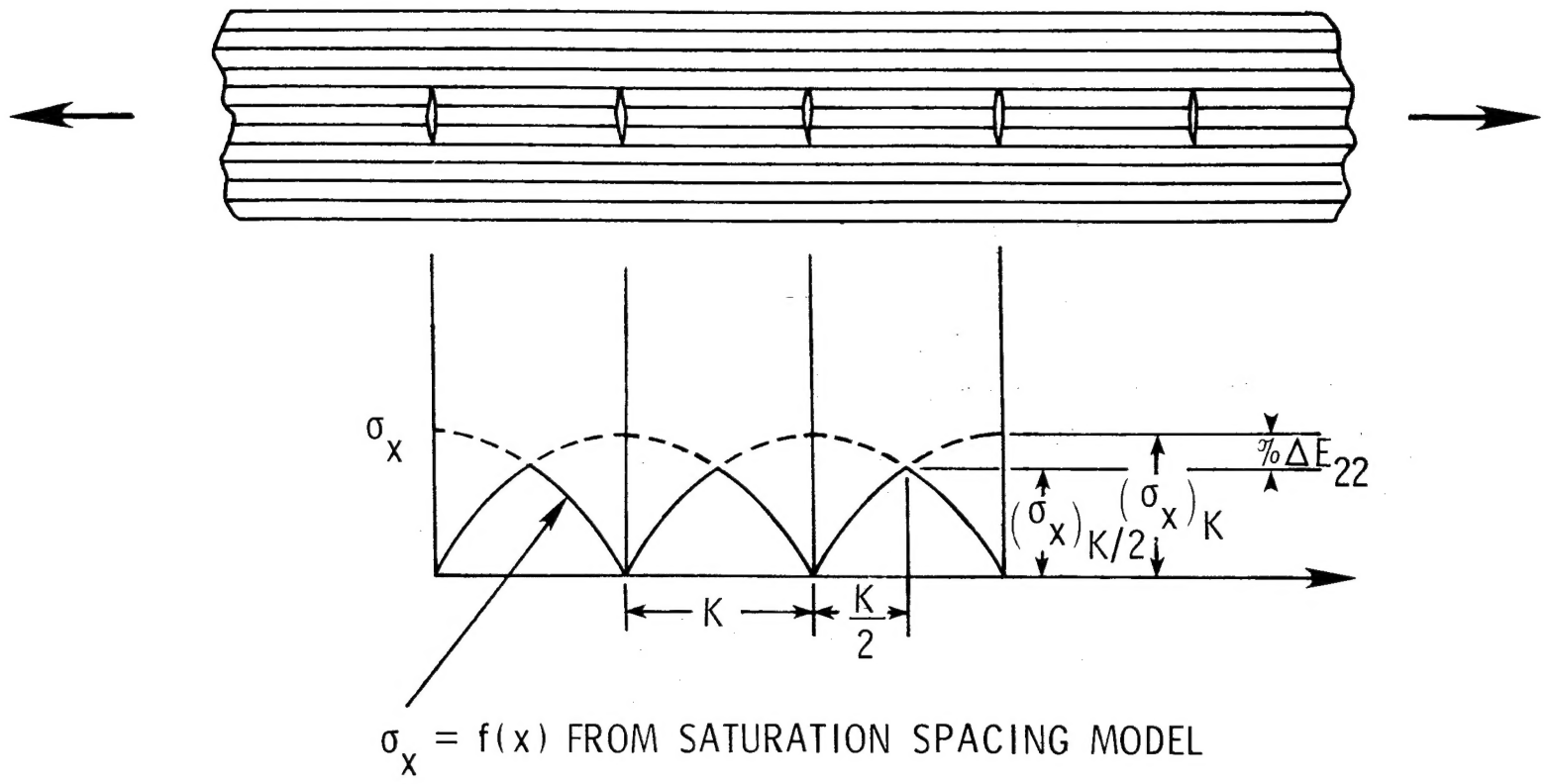

Figure 23.- Estimate of stiffness loss from 90° ply cracks.

1. Report No.	2. Government Accession No.	3. Recipient's Catalog No.
NASA TM-81940		

4. Title and Subtitle	5. Report Date
CHARACTERIZATION OF DELAMINATION ONSET AND GROWTH IN A COMPOSITE LAMINATE	January 1981
	6. Performing Organization Code
7. Author(s)	8. Performing Organization Report No.
T. Kevin O'Brien	
9. Performing Organization Name and Address	10. Work Unit No.
NASA Langley Research Center Hampton, VA 23665	506-53-23-05
	11. Contract or Grant No.
	13. Type of Report and Period Covered
12. Sponsoring Agency Name and Address	Technical Memorandum
National Aeronautics and Space Administration Washington, DC 20546	14. Army Project No.

15. Supplementary Notes

Presented at the ASTM Symposium on Damage in Composite Materials: Basic Mechanisms, Accumulation, Tolerance, and Characterization, Bal Harbour, Florida, November 10-14, 1980.

16. Abstract

The onset and growth of delaminations in unnotched $[\pm 30/\pm 30/90/\overline{90}]_s$ graphite-epoxy laminates is described quantitatively. These laminates, designed to delaminate at the edges under tensile loads, were tested and analyzed. Delamination growth and stiffness loss were monitored nondestructively. Laminate stiffness decreased linearly with delamination size. The strain energy release rate, G, associated with delamination growth, was calculated from two analyses. A critical G for delamination onset was determined, and then was used to predict the onset of delaminations in $[+45_n/-45_n/0_n/90_n]_s$ (n=1,2,3) laminates. A delamination resistance curve (R-curve) was developed to characterize the observed stable delamination growth under quasi-static loading. A power law correlation between G and delamination growth rates in fatigue was established.

17. Key Words (Suggested by Author(s))		18. Distribution Statement
Graphite-epoxy	Stiffness loss	Unclassified - Unlimited
Delamination	R-curve	
Ply cracking	Fatigue	Subject Category 24
Rule of mixtures	Growth law	
Strain energy release rate		

19. Security Classif. (of this report)	20. Security Classif. (of this page)	21. No. of Pages	22. Price*
Unclassified	Unclassified	60	A04

*For sale by the National Technical Information Service, Springfield, Virginia 22161